uc3m | Universidad Carlos III de Madrid

Bachelor's degree in Biomedical Engineering

2017-2018

Bachelor thesis

"Cardio-respiratory monitor with synchronization capabilities"

Sarah Rance López

Tutor

Juan José Vaquero López

Leganés, October 10th, 2018

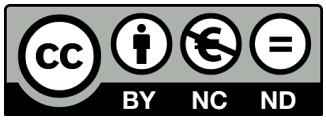

ABSTRACT

Cardiopathies are some of the most common causes of death worldwide and therefore cardiac imaging is one of the most important studies that can be performed in the diagnostic process. However, not only does cardiac imaging have special requirements when it comes to the equipment used such as spatial and temporal resolution, but final image quality and therefore diagnosis may be greatly hindered by the movement of the thoracic cavity and of the heart itself.

The problem of motion artifacts caused by breathing motion together with heart movement during the cardiac cycle is solved by image gating, by synchronising vital signs to an image acquisition system, and obtaining images according to the generated signal, and therefore reducing movement artifacts.

To address this issue, the objective of this bachelor thesis is to propose a prototype for the implementation of a cardio-respiratory monitor designed, developed and programmed for image gating in a preclinical setting. This device was built with an Arduino microcontroller, an ECG-FE, a pressure sensor connected to a pressure transducer to sense the respiratory signal, a touchscreen and a rectal temperature sensing module. All signals are sampled and processed by the Arduino MEGA 2560 microcontroller.

The testing of the prototype was performed with simulated patients in *UC3M* laboratories, and with small animals at *Hospital General Universitario Gregorio Marañón's Laboratorio de Imagen Médica y Cirugía Experimental.*

Overall, results were very satisfactory despite an issue with missed TTL beats that will be resolved in future work by redesigning the algorithm for touchscreen visualisation of the different signals, and gating conditions.

The reduced costs of this device with respect to other such devices on the market, along with the intuitive interface and its portability could ease implementation of image gating, enabling key preclinical research for heart disease.

Keywords: Gated imaging device, ECG, respiration, microcontroller, TTL.

ACKNOWLEDGEMENTS

First of all I would like to thank Juan José Vaquero, for his help, support and encouragement throughout. Without his guidance, this bachelor thesis would not have been accomplished.

I would also like to show thanks to all the people from the *"Departamento de Ingeniería Biomédica y Aeroespacial"* who have helped me with the project. Guillermo Vizcaíno deserves a heartfelt thank you for everything he has done for me: not only helping me with the most technical aspects of the project, but also encouraging me every step of the way. Alberto and Miguel have also provided help and guidance whenever I needed it.

Assistance and input provided by the staff of the *Laboratorio de Imagen Médica y Cirugía Experimental* was greatly appreciated.

However, this project has needed more than just academic and technical support, also a lot of patience and understanding. I wish I had better words to thank everyone who has helped me in one way or another.

To every member of the group *Chicuelas*, that have always been there no matter what, and have shown unwavering support whenever needed. You have helped me both intellectually and personally, and I am very grateful to each and every one of you.

And last but not least, to my family, without whom this would not have been possible.

CONTENTS

LIST OF FIGURES

LIST OF TABLES

1. THEORETICAL BACKGROUND

This section presents and explains the theoretical background of the various aspects of the project.

1.1. Heart and electrocardiography fundamentals

Oxygen distribution has been one of the main driving forces of evolution, and among the organs that play a critical role in respiration effectiveness is the heart. The heart is a highly specialised cone-shaped muscle that constitutes the main organ of the circulatory system. It is located inside the mediastinum, between the lungs, and anterior to the spine. Its main function is to pump blood throughout the body and, to do this, it requires a very potent and coordinated muscular action, achieved through the innervation and the electric activity of the cardiomyocytes [1] [2].

The heart is divided into four different chambers (see Fig. 1.1): the two upper ones are the atria that serve as a receiving chamber for all the blood that has returned to the heart and the two lower ones are the ventricles, that pump the blood throughout the body. On the left side of the heart, the left atrium and ventricle receive and pump oxygenated blood coming from the lungs to the rest of the body; while at the same time in the right side, the right atrium and ventricle receive and pump deoxygenated blood coming from the organs to the lungs (called pulmonary circulation) [1] [3].

These events happen in a well-synchronised rhythmical manner defining the cardiac cycle. First, the heart is in a period of relaxation called diastole. Blood accumulated in the atria flows passively through the atrioventricular valves to fill the ventricles. At the end of diastole, both atria contract to propel additional blood just before the atrioventricular valves close. In a second stage, diastole is followed by a period of contraction called systole in which ventricles expel blood out of the heart [2].

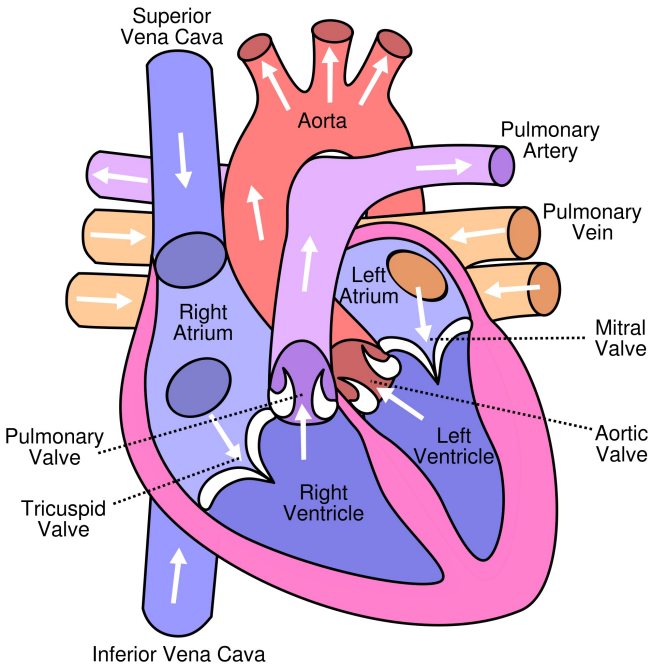

Fig. 1.1. Heart anatomy diagram [4]

1.1.1. Electrocardiogram (ECG)

There are many types of test to characterise an animal's heart and heart rate, among which echocardiography and arterial pressure are two of the most relevant. These methods are used to calculate parameters such as heart rate but most of these methods cannot distinguish whether a heart beat is ectopic[1] or not. This is why electrocardiography has become the diagnosis standard for cardiopathies [5].

The electrocardiogram (ECG or EKG) is the measurement, through a series of electrodes placed on the skin, of the voltage produced by the electrical activity of the heart. It shows the sequence of cardiac events and can provide information about the atria and ventricle size, as well as almost any cardiopathy a patient may suffer from [6].

The ECG can be intuitively understood as the sum of the voltages throughout the heart along time and along a direction, the electrical axis. A healthy ECG has a particular shape and positioning of the waves that make up the signal, and any alteration of this pattern could mean the presence of a heart abnormality.

The resulting signal is made up of several different components: the P-wave, the QRS complex, and the T-wave [7] [2].

[1]Ectopic is a term that describes any disturbance in the electrical conduction system of the heart

In Fig 1.2 the following characteristic components of a healthy ECG can be seen:

- **P-wave**: is the depolarization of the atria. The initial rise of the wave corresponds to the depolarization of the right atrium and the posterior fall of the wave represents the depolarization of the left atrium.
- **QRS complex**: corresponds to the repolarization of the atria (which cannot be seen in a normal ECG), at the same time as the ventricles depolarize and contract.
- **Q wave**: represents the action potential travelling along the septum[2] of the heart.
- **R and S waves**: indicate the contraction of the ventricles.
- **T wave**: represents repolarization of ventricles, it is usually a positive wave. Sometimes a deviated ST segment (the signal connecting the QRS complex with the T wave) can be indicative of serious cardiopathies such as ischemia or myocardial infarction.

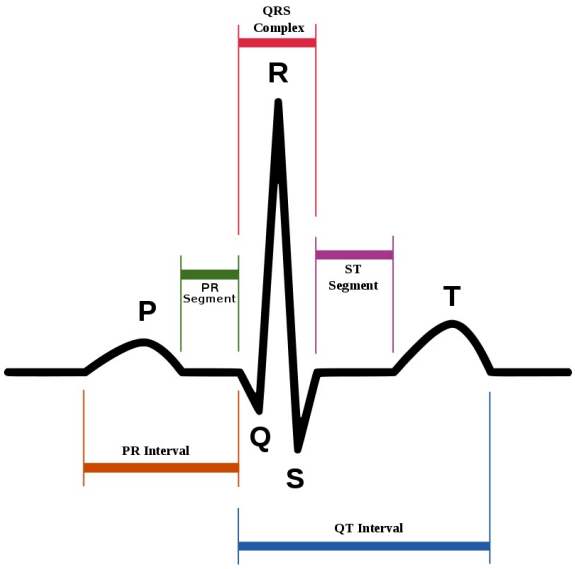

Fig. 1.2. ECG graph with a normal sinus rhythm [8]

By placing electrodes on the patient's skin we can obtain several different configurations of ECG, allowing physicians to diagnose conduction and rhythm disturbances along different directions according to the lead positioning, by performing the substraction and grounding of several different leads [2].

Leads of the ECG are:

[2]Septum: wall dividing both sides of the heart

- **Lead I**: measures the difference of potential between the electrode on the right arm and the left arm.
- **Lead II**: measures from right arm to left leg.
- **Lead III**: measures from left arm to left leg.

These three leads conform Eindthoven's triangle, and these in turn can be combined in the following way to obtain the augmented leads [2]:

- **aVR (augmented vector right)**: considers the right arm electrode to be positive, while the negative electrode is a combination of the left am and the left leg. It augments the effect of the right arm.
- **aVL (augmented Vector Left)**: has the positive electrode in the left arm, while the negative one is a combination of the other two leads.
- **aVF (augmented vector foot)**: considers the positive electrode to be the one placed in the foot, augmenting its effect on the overall signal.

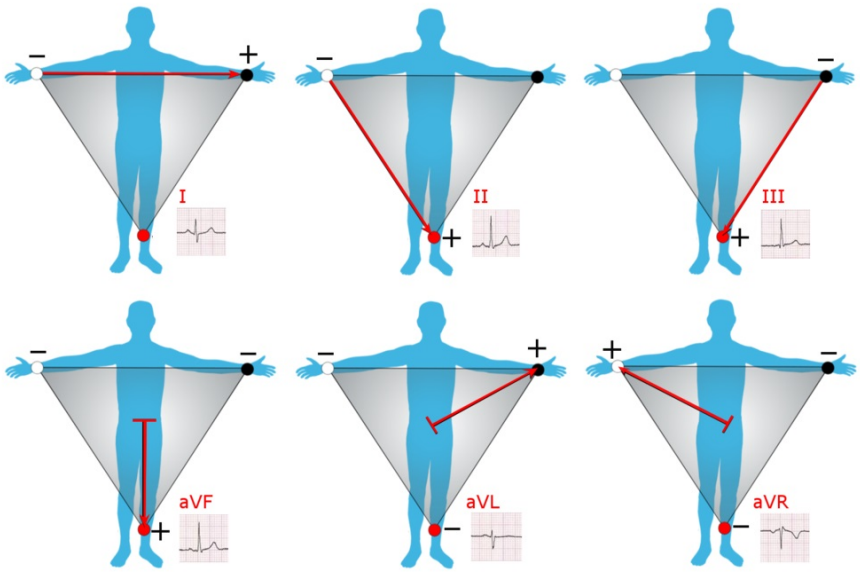

Fig. 1.3. The limb leads and augmented limb leads [9]

Real time detection of the QRS complex is one of the most challenging issues within devices for ECG monitorization. Sources of noise may affect detection capacity, and a sufficiently accurate and stable algorithm is necessary [10].

1.1.2. Bio-electrical ECG signal processing

The ECG has many possible sources of either noise or artifact that cause the signal to be distorted. The three most common sources of noise are the following [11]:

Baseline Wander

Baseline wander is a low frequency noise that is introduced into the signal. It can be due to body movement, respiration or perspiration (that will cause variations in electrode impedance, and distort the acquired signal).
It has very low frequencies (usually under 1 Hz), and it can be eliminated with the implementation of a high pass filter with a very low cutoff frequency, usually 0,5 Hz [12]. These filters can be analogue, digital time-invariant high pass filters or digital adaptive filter to eliminate baseline wander according to the frequency content of the current signal.

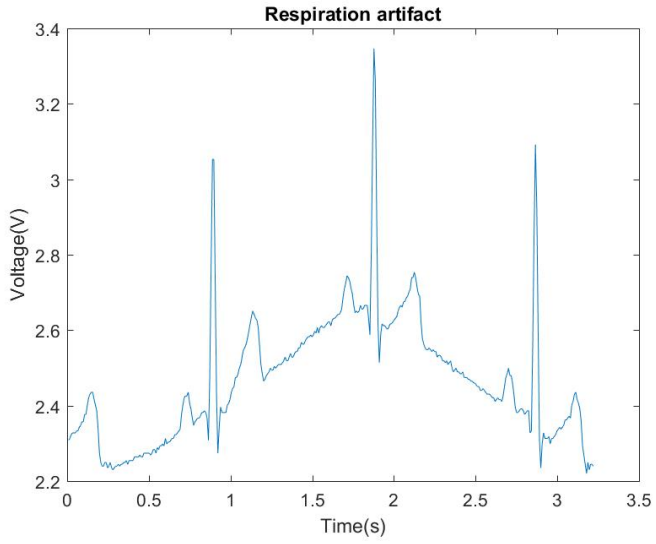

Fig. 1.4. Example of baseline wander artifact introduced by chest movement where a full respiratory cycle of inhalation and exhalation is visible.

Power line interference

The power line interference in a signal is caused by the frequency inherent to power administration of a device. The most common frequencies for this types of noise are 50

Hz for Europe and 60 Hz for North America. Unlike the other two types of noise, it is periodic, and can be perceived as the sum of a sinusoid of this frequency to the original ECG signal, causing a thick and unreadable signal (seen in Fig. 1.5) [12].

The main solution for this type of interference is the introduction of a notch filter, that will remove as narrow a frequency band as possible, causing little distortion to the signal of interest [11].

However, this type of noise can be avoided by using a battery. The presence of an autonomous power source eliminates the need of using a power line all together, and batteries do not have an inherent frequency, meaning that they will not be a source of noise.

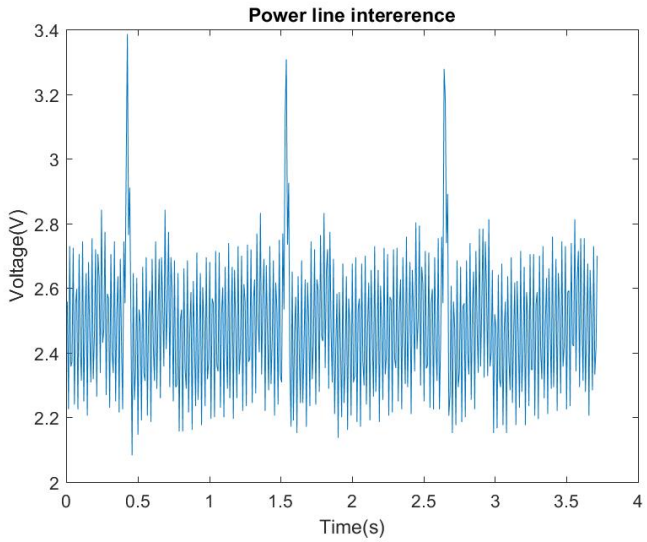

Fig. 1.5. Example of 50Hz noise introduced into a 60 beats per minute signal

Electromyographic/Muscle Noise

Muscle movement is a major source of noise that can alter the signal, as muscle contraction introduces a high frequency noise in the resulting signal [12].

It can be avoided by introducing a low pass filter in the acquisition process, eliminating those frequencies higher than the cutoff. This processing is specially critical when it comes to wearable devices, and may be especially difficult when treating species whose basal heart rate is relatively high.

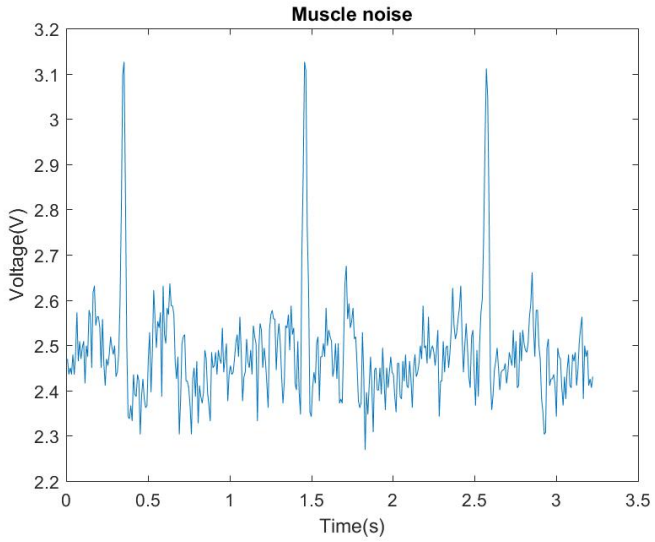

Fig. 1.6. Example of signal read with muscle noise introduced into a 60 beats per minute simulated ECG signal

1.1.3. Human and rodent cardiac characteristics

Humans and mice have very similar heart anatomies and as such will have comparable parameters of the ECG. However, the most notable difference is the heart rate. Heart rate is greatly dependent on parameters such as output volume, and physiologic condition of animals, as well as on environmental factors such as activity levels and time of day [13]. Some medical conditions can severely affect the ECG. Anaesthetised animals can greatly decrease their heart rates, so that the values in table 1.1 greatly depend on the conditions of the animal [14].

Species	Minimum heart rate	Maximum heart rate
Human [15]	40	100
Rat [16]	330	480
Mouse under anaesthesia [14]	320	480
Wild-type Mouse [5]	500	700

TABLE 1.1. AVERAGE MAXIMUM AND MINIMUM HEART RATES IN BPM FOR DIFFERENT SPECIES

1.2. Fundamentals of respiration

Oxygen distribution not only depends on circulation, but also on respiration, which is another factor that has greatly driven specialisation.

The respiratory system is made up mainly of airways (trachea, bronchi and bronchioli) and lungs. Lungs are two organs of spongy texture consisting mainly of alveolar ducts and alveoli, where gas exchange occurs. They are subdivided into lobes and segments [17].

In mammals, the driving force behind the respiration is the relaxation and the contraction of the diaphragm and the intercostal muscles. It is the creation of a net pressure on the lungs by these muscles that causes inspiration and exhalation to occur, causing chest movement.

In a resting position, when the body performs the so-called quiet breathing, intrapulmonary pressure and atmospheric pressure are balanced at 760 mm Hg [18], so air will only access the lungs when the intrapulmonary pressure decreases, a change generated by an increase in volume of the thoracic cavity. This is called inspiration: the diaphragm and the external intercostal muscles both contract, causing a 1 mm Hg difference with the atmospheric pressure, allowing pulmonary ventilation to occur.

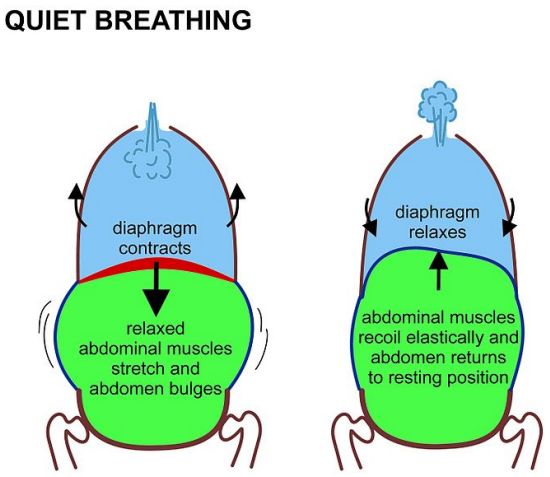

Fig. 1.7. Quiet breathing mechanism. Inhalation on the left, exhalation on the right. Red indicates contracting muscles, relaxed muscles are shown in blue [19]

The opposite process, exhalation, is produced by the relaxation of these muscles,

consequently reducing the volume of the thoracic cavity and causing a positive pressure with respect to the atmosphere, driving the gas out of the lungs.

1.2.1. Respiratory signals

There are several ways to measure respiration in literature, one of the most commonly used methods for monitoring respiration is pulse oxymetry, however, this signal does not directly reflect movement of the chest, but blood oxygen saturation [20].
The most commonly used signals representing non invasive measurements that reflect the inspiration and exhalation or chest movement are:

Impedance pneumography

Impedance pneumography measures changes of trans-thoracic impedance with chest volume changes. It is performed by transmitting a high frequency signal through the body and examining the dephasing of this signal between input and output of the body. This dephasing can be used to reconstruct the respiratory cycle signals [21].
The difference in impedances can usually be attributed mainly to the difference in conductance paths between the expanded thoracic cavity and the resting state [22].
However, this technique possesses unique requirements for the electrodes, such as surface area and materials needed [23].

Electrocardiogram (ECG) derived respiration (EDR)

As mentioned previously, baseline wander in ECGs can be caused by respiratory motion, because of the different positioning of the electrodes with respect to the heart along time, caused by breathing [24] [20].
It can be understood as respiration modulation in the direction of the cardiac axis, seen in figure 1.8.

Fig. 1.8. Respiration-induced modulation of QRS amplitude [24]

Temperature sensitive respiration sensing

A temperature sensitive resistor placed near the nostril of the animal enables the sensing of changes of temperature in air between exhalation and inspiration. By reading the temperature measurements, users are able to interpret whether the animal is breathing in or out, and thus completely reconstruct the breathing cycle of the animal [25].
Other techniques based on temperature detection include sensing through the thermal imaging of the facial features related to respiration of the subject [20].

Pressure sensitive detection

Pressure sensitive detection measures changes in pressure that the chest causes when the body is compressed against a sensor. It can be implemented, among other options, with a force-sensitive-resistor, or with a pressure sensor. This category also encompasses the sensors that are placed in ventilation tubes or cannulae [20], and piezoelectric sensing [26].

Many other approaches are available for measurement of the respiratory rate, such as strain sensing implementations, commonly used for thoracic belts, or optical based systems [20].

1.2.2. Human and rodent respiratory characteristics

Breathing rate is severely affected by conditions such as distress or physical condition, and as with heart rates, anaesthesia can also have considerable impact on the rate of

respiration.

Species	Minimum respiration rate measured in CPM	Maximum respiration(CPM)
Human (quiet breathing) [15]	15	20
Rat [16][27]	85	120
Mouse [28]	80	230

TABLE 1.2. AVERAGE MAXIMUM AND MINIMUM RESPIRATION RATES FOR DIFFERENT SPECIES

1.3. Image gating

As previously discussed, cardiac imaging is especially sensitive to cardiorespiratory motion artifacts. To avoid this type of artifact, cardiac and/or respiratory signals can be synchronised with an image acquisition system. This technique is called gating, and the images it produces are called gated images [29].
It can be applied to any imaging modality, from X-Rays to Ultrasound. The most commonly used variation of this technique is cardiac gating, a technique that can help provide a more in depth-knowledge of the heart's cycle, through the synchronisation of the ECG, yielding information of the stage of the cardiac cycle of each of the images.

1.3.1. Types of gating according to acquisition synchronisation

There are mainly two modalities of synchronisation with imaging systems: prospective and retrospective gating.

Prospective gating/triggering

The terms prospective gating and triggering are interchangeable, and they refer to the systems where the acquisition of the image only occurs after the detection of a certain event, such as the R-wave in the ECG, or the momentary absence of thoracic movement [30].

Retrospective gating

In retrospective gating, images are continuously acquired, there is no response to trigger. Instead, ECG or respiration signals are acquired along with the images, and these signals can be taken into account when the study is reconstructed, through several processing techniques [30].

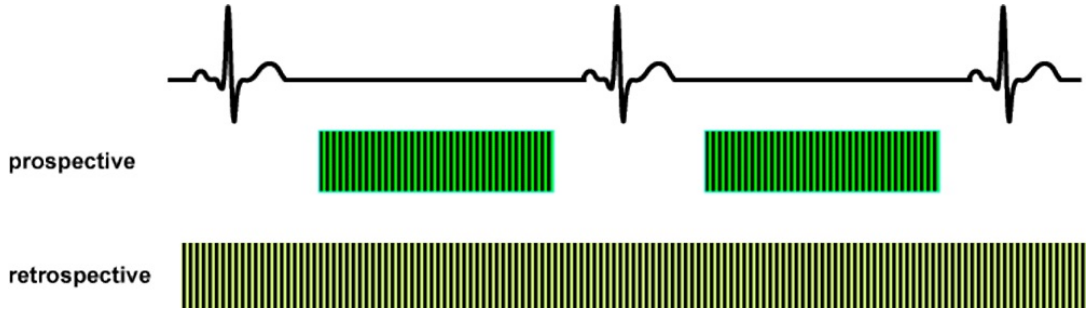

Fig. 1.9. Differences between acquisitions of prospective and retrospective gating. Courtesy of Allen Ellster [30]

1.3.2. Types of gating according to signals used

Cardiac gating

Cardiac cycles can be sensed with many different strategies for image gating, the most common and reliable of which is the ECG. Peripheral pulse transducers may be used but are considered to be unreliable because of the lag that they may have with respect to the heart, therefore they are not commonly used for cardiac studies [31].

Respiratory gating

Thoracic expansion during respiration may affect the image acquisitions of both the thoracic region and the abdomen. One of the techniques most commonly used for respiratory signal acquisition is the use of a thoracic belt, a device placed around the chest of the subject to sense respiratory movement [31].

2. INTRODUCTION

2.1. State of the art and previous work

There are plenty of devices on the market that can provide solutions to the problem of gating, as well as give constant monitoring. Most of them have common features such as cardiac (ECG) monitoring, a variety of approaches to respiration measurements, and an output TTL signal, which allows them to be directly connected to an imaging machine, to obtain a gated image study.

Fig. 2.1. Argus PET-CT at *Laboratorio de Imagen Médica y Cirugía Experimental* at Hospital Gregorio Marañón.

At the *"Laboratorio de Imagen Medica y Cirugía Experimental"* they use an *Omicron Vision Pet* monitor by RGB, connected to the Argus PET / CT, and although this device provides an excellent synchronisation signal to obtain a gated image, researchers and technicians have both shown interest in a smaller, more portable device that could be used in the procedures where the more advanced features of the previously mentioned device are not necessary.

This bachelor thesis was initially conceived as the continuation of two previous theses: the first one [32] proved that such a device could be used by employing only the elec-

trocardiography signal, and the second one [33] refined both the architecture and the software of the device.

The first bachelor thesis to approach the subject was finished in 2014, can be seen in Fig. 2.2, and its main objective was to use a microcontroller to achieve a prospective gating device for image gating from a cardiac signal. It also aimed to miniaturise device present in the *"Laboratorio de Imagen Médica"*. This implementation was achieved with an Arduino Uno and a ADS1298 ECG Front End by Texas Instruments, and a Gameduino 2 screen. However, its use was not intuitive and its refinement required further work [32].

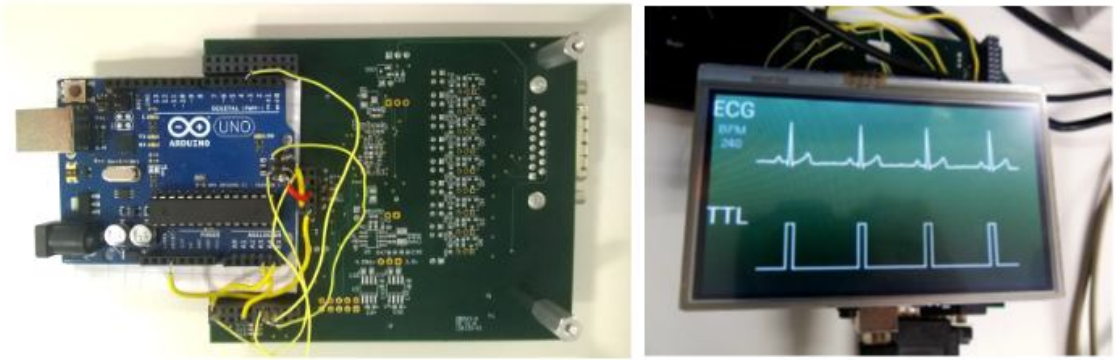

Fig. 2.2. Initial proof of concept for the gating device. Reproduced with permission from [32]

The second bachelor thesis that approached the subject had, as a main goal, the more robust and stable implementation of the previous proof of concept, by substitution of the Arduino Uno with a microcontroller with a larger SPI bus, as well as introducing new aspects to the project like the measurement of the rectal temperature, and a more refined user interface [33].

These modifications made the device more robust and portable than the first approach, as can be seen in Fig. 2.3.

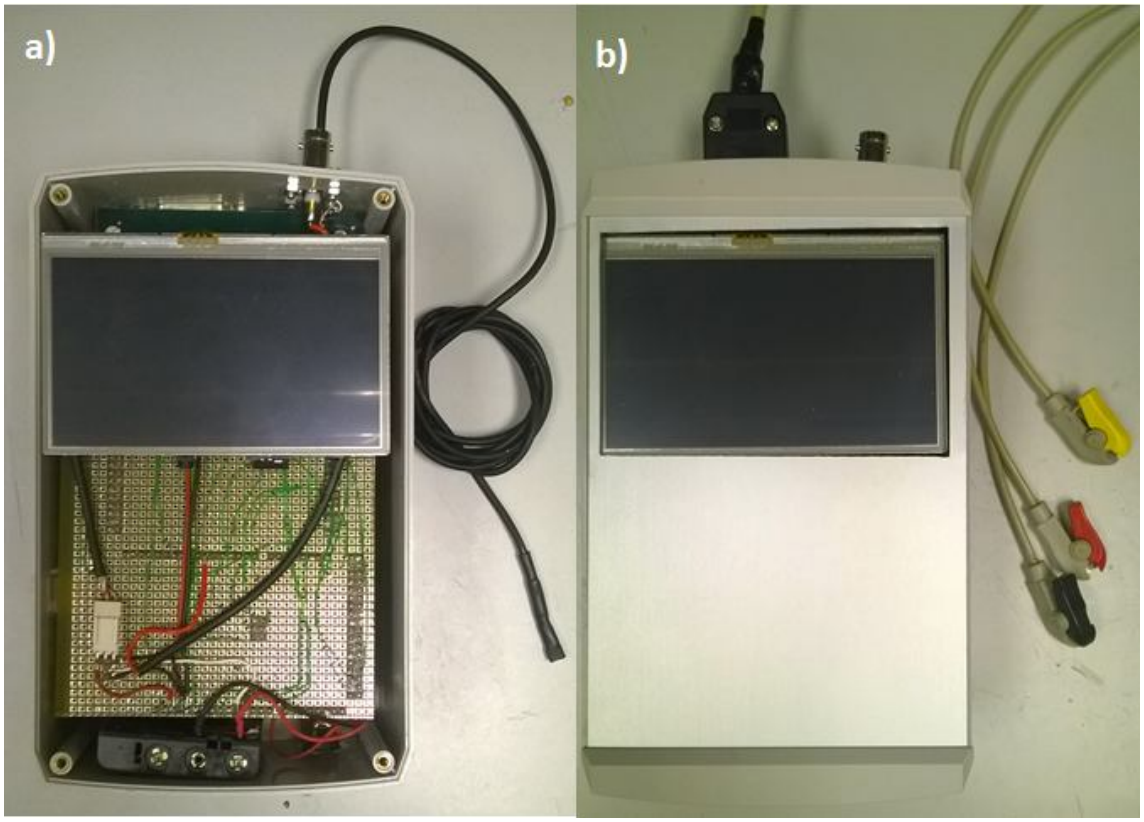

Fig. 2.3. Previous bachelor thesis final architecture for the device, both without the final aluminium cover (a) and with the cover for the final device (b). Reproduced with permission from [33]

The aim of this bachelor thesis is to completely redesign the architecture of the device in order to include the respiration signal, a feature that both previous devices lacked. This addition also required the introduction of a menu to select the gating mode for the current image acquisition.

2.2. Regulatory framework

This project's experimental work was performed under the strict guidelines for animal experimentation that Spanish and European Law regulate, as well as the protocols set in place at the *"Laboratorio de Imagen Médica"* at the *"Hospital General Universitario Gregorio Marañón"*.

All animal procedures and housing were previously approved by the Animal Experimentation Ethics Committee of Hospital General Universitario Gregorio Marañón, Madrid, Spain and performed according to current legislation (Real Decreto 53/2013 (39) and

86/609/EEC).

Before the commercialisation of the device, further studies should be carried out to ensure compliance with both Spanish and European regulation for medical devices: Royal decree 1591/2009, and Council Directive 93/42/EEC on Medical Devices (MDD)(1993) respectively.

2.3. Motivation

Medical practice benefitted hugely from the discovery of X-rays more than a century ago. Nowadays physicians have a wide range of imaging tools at their disposal to aid diagnosis: planar X-ray, computed tomography, magnetic resonance imaging, positron emission tomography, and many other modalities. This range of tools is used to characterise the body of humans and animals alike.

However, one of the main and most common problems of imaging is motion artifact, and many efforts are being made to solve this issue. Instead of applying filters after the acquisition of the image, external devices can be introduced to monitor the patient's vitals signs and use these signals to make the acquisition process more accurate, which is what the gating process relies on.

Cardiac imaging is one of the most complicated operations within the medical imaging field. Not only does it require a high spatial resolution due to the small structures that this type of imaging is addressed to, but also a high temporal resolution, due to the need for a lack of motion artifacts, and the big range of values that the heart rate may take depending on the species.

The current CT techniques target this level of temporal resolution with the use of specific ECG-synchronised techniques, segmentation, and tailored reconstruction algorithms. Respiratory motion must also be eliminated for cardiac imaging, so scanning is optimally performed in a single breath-hold.

The main motivation behind this bachelor thesis is to provide a suitable solution for this problem using gated imaging. This device is aimed to be used at the Hospital General Universitario Gregorio Marañón where there is a need of reducing motion blurring in the images taken with the Argus CT/PET machine (Sedecal, Madrid) in cardiac studies.

2.4. Objectives

The main objective of this project is the design, development and programming of an electronic device that allows the monitoring of the ECG and the respiration signal of small animals, and can consequently provide an adequate gating signal for the Argus PET/CT machine of the *Laboratorio de Imagen Médica y Cirugía Experimental* at the Hospital General Universitario Gregorio Marañón.

Further objectives for the project are as follows:

- The achievement of a low cost device that is simple to use, compact, and convenient for the technicians and researchers at *Laboratorio de Imagen Médica y Cirugía Experimental* at the Hospital General Universitario Gregorio Marañón.
- Improving the hardware and software functions of the prototype device from a previous bachelor thesis, making it easier to use, more intuitive and ultimately provide a fuller range of functionality, through the creation of a touchscreen interface that will enable the user to select the gating mode and ease communication with end users.
- To appropriately sample cardiac activity of mice: sampling the ECG signal with a frequency content sufficient to achieve a satisfactory gating signal, while approaching real time monitorisation of the small animal's vital signs.
- The inclusion of the respiration signal of the animal to the previous project, which will require the addition of another gating mode to the device.
- To substitute the previous project's temperature sensor for a more appropriate sensor for use in small animals, with an easier preclinical implementation, and an equally reliable measurement.
- Perfecting screen function to enable visualisation of an adequate duration of the signals present on the screen, together with an optimum refresh time of the screen.
- To adjust sampling of the signals according to the frequency content of each one, to sufficiently sample them, and provide a more efficient TTL signal.

- To obtain a clean ECG signal eliminating possible sources of noise that may cause a mistaken TTL activation.
- Testing the device in a real preclinical environment with small animals and ensuring its correct operation with the existing hospital hardware.

2.5. Thesis structure

The structure of this thesis is coherent and logical. Firstly, I present a theoretical background on some of the topics discussed in this thesis, including electrocardiography basics, respiration, and characteristics of respiratory signals. This constitutes the backdrop for the concept of imaging gating, and provides the necessary information for the understanding of the rest of the thesis.
Secondly, in the introduction, the previous work state of the art is stated, as well as the motivation and the objectives of this project.
The explanation of the materials used during the development of this thesis constitutes the third section of this document, including brief explanation of the function of each component within the final arrangement of the device.
The final arrangement of both software and hardware is discussed in the following section, to explain the interaction of the different components and completely describe the final setup of the device.
The fifth section presents the experimental results of the prototype, to ascertain whether the objectives have been achieved. Subsequently, this document reviews the different aspects of the current status of the device and revises its future improvements.
The estimated budget of this project is also included.

3. MATERIALS

3.1. ECG device architecture

The small-size ECG monitor consists of six main components: the microcontroller board Arduino MEGA2560, the AD8232 front end for cardiac measurements, the VMA412 TFT screen, the pressure sensor MPXV5010GC7U, the temperature sensor P1K0.161.1E.A.040, and the BNC connector. All these parts are electronically connected through an adapter protoboard. The ensemble is encased in an ABS insulated box with a removable aluminium front (Fig. 3.1 left with the aluminium front, and right without the cover) with input and output connectors that enable the device to be interfaced with the imaging machine and with a computer if necessary.
This box also encases the voltage supply to make the device autonomous.

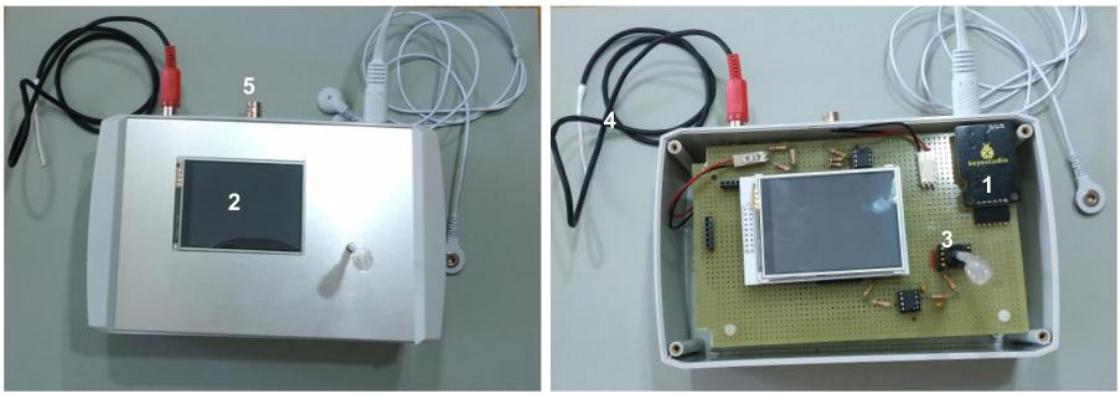

Fig. 3.1. Complete architecture of the device: the AD8232 front end for cardiac measurements (1), the VMA412 TFT screen (2), the pressure sensor used for respiration (MPXV5010GC7U) (3), the temperature sensor P1K0.161. 1E.A.040 (4), and the BNC connector (5)

Figure 3.1 shows the complete architecture of the device, with all cables necessary for monitorization.

3.1.1. Arduino MEGA 2560

The Arduino Mega 2560 is an open source hardware microcontroller board based on the ATmega 2560 chip that contains a processor core, memory (a flash memory of 256 KB, and 8KB of SRAM), and programmable input/output peripherals in an integrated circuit. Arduino Mega 2560 has a USB connector for ease of interface with the computer, a power jack, and a reset button. It also has a total of 80 pins with different functions which can handle different types of input and output signals, like PWM, analog or digital signals.

3.1.2. Ks0261 AD8232 ECG Measurement Heart Monitor Sensor Module

The Ks0261 AD8232 ECG Measurement Heart Monitor Sensor Module by Keyestudio, is specially designed to filter and process signals in order to monitor heart rate. It is also conceived for use with Arduino projects.

Fig. 3.2. Ks0261 AD8232 ECG Front End

3.1.3. VMA412

The VMA412 manufactured by Velleman is a touchscreen compatible with Arduino. It has capacity to show up to 262.000 colours and is easily adaptable to Arduino projects. Its connections are specially designed for direct contact to Arduino UNO and Arduino MEGA boards.

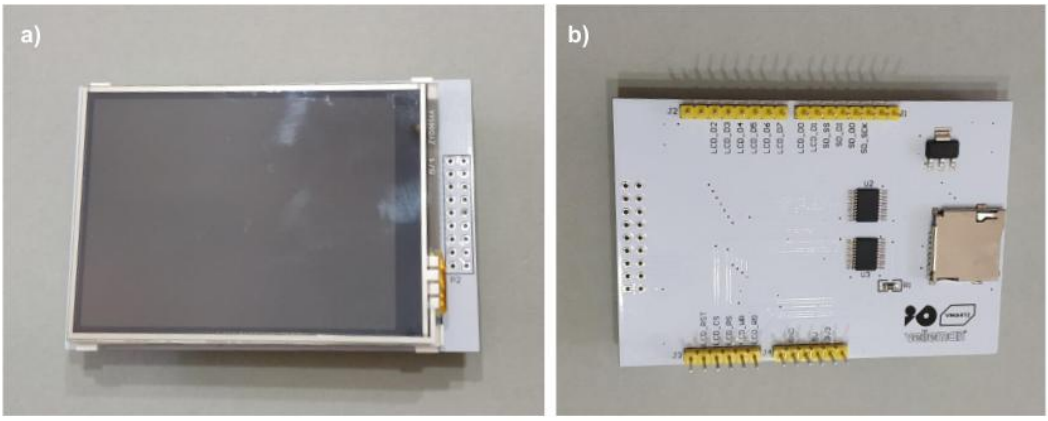

Fig. 3.3. Front (a) and back (b) views of the VMA412 screen.

3.1.4. Temperature sensor: P1K0.161.1E.A.040

This temperature sensor has the optimal size for applications that require a sensor that is both small and accurate. It also possesses an excellent long-term stability, fast response time, and is specially designed for low self-heating.

The sensor was encased in a medical-grade tube obtained from the hospital, and fixed by application of silicone, as seen in Fig. 3.4, a material easily sterilized and biocompatible. This silicone was specially chosen for its fluidity and its thermal conduction properties. On the opposite end of the cable, an RCA connector was used to interface with the device.

Fig. 3.4. Temperature sensor setup

3.1.5. Pressure sensor: MPXV5010GC7U

The pressure sensor used for this application is an integrated silicon pressure sensor made by NXP USA Inc, recommended specially for hospital applications and respiratory devices (seen in Fig. 3.5). It is a gauge pressure sensor, detecting between 10 and 40 kPa, guaranteeing better precision for detection of small pressure changes than that of other products on the market. The output varies between 0.2 V to 4.7 V, an optimal range for sampling with Arduino microcontrollers.

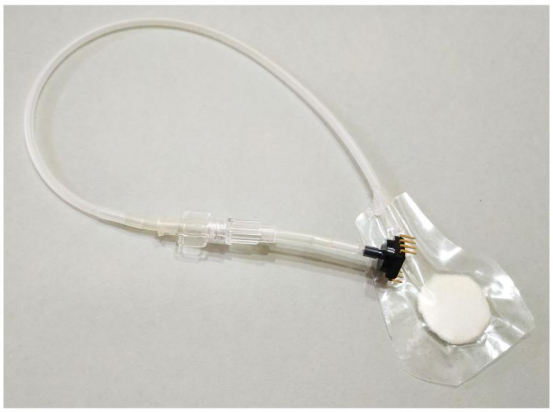

Fig. 3.5. Pressure sensor setup: the pressure sensor connected to the *Luer* lock used to connect to the manufactured or the hospital pressure transducer to sense respiration.

These characteristics make it an ideal pressure sensor for use with Arduino microcontrollers. A medical-grade tube was connected to the sensor in order to add the *Luer* lock that provides adaptability to the pre-existing hospital setup.

3.1.6. Connector protoboard

The connector protoboard has the standard hole dimensions for interaction with Arduino boards as well as for most of the components used for this project: hole diameter of 1 mm, and hole distance of 2.54 x 2.54 mm, that of standard through-hole mounts.

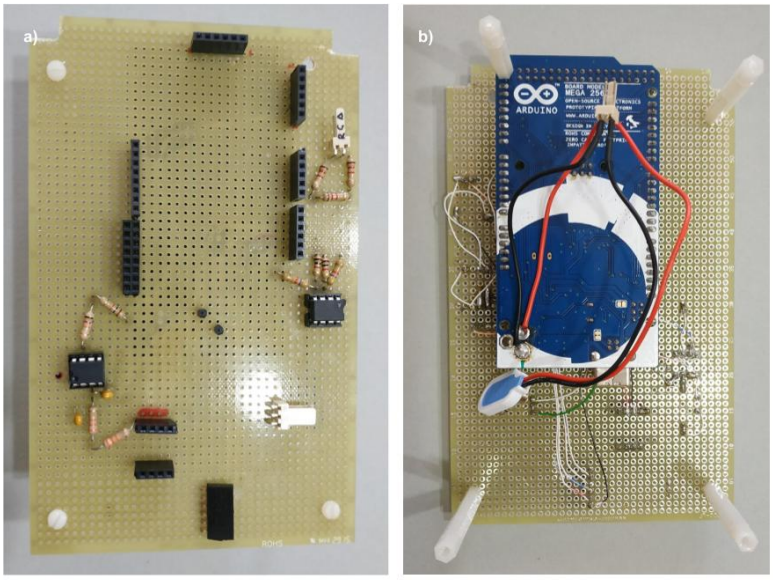

Fig. 3.6. Front and back views of the connector protoboard, with the Arduino Mega connected.

3.1.7. Resistors and capacitors

For the filtering circuits, resistors and capacitors are needed. Annex B is a comprehensive list of the components used.

3.1.8. Other components

Enclosure box

In order to build a robust ECG device all the previous components have to be assembled together and contained in a plastic box embedded with all the complements necessary for power and input/output connectivity.
The enclosure box used is the RETEX model Series 103 P 33103005 with the following dimensions 190 x 115 x 72 mm. It is made of ABS plastic and has an aluminium front.

Cables

Three lead electrodes of two different types were used for recording either the simulated or biological ECG input signals during the testing of the device.
For the simulated signals, the cable used was provided specially for the ECG FE (Fig.

3.7-a.). However, small animal tests required the use of miniaturised needle electrodes, which were specially made with a low input impedance and a stereo Jack connector (Fig. 3.7-b.).
The interface between the imaging machine and the device was provided by a BNC male cable.

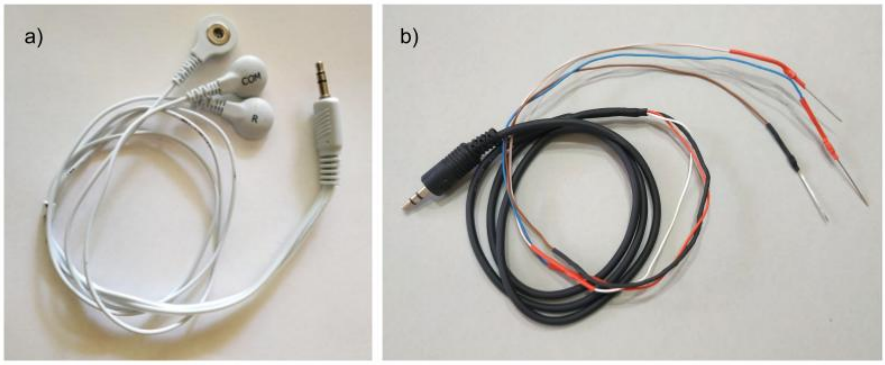

Fig. 3.7. Cables used for the ECG front end.

Power supply

A 9V battery was used as a power source to make the device portable. A complementary power switch was also installed on the box to turn the power supply on or off.

3.2. Testing and programming instruments

3.2.1. Pro-sim 8 simulator

Pro Sim 8 vital signs simulator by Fluke Biomedical is an eight-in-one multifunction patient simulator, being capable of simulating ECG, respiration, temperature and sPO2 among other signals. This simulator allows modification of parameters such as axis, amplitude, and heart rate.
Parameters such as waveform group, axis or amplitude can be modified within the simulator. It is worth mentioning that the range of heart rate is between 10 and 360 BPM in 1 BPM steps. This range makes it suitable for rat heart rate simulation, but insufficient for mice simulation.

Fig. 3.8. Pro-sim 8 simulator options (above), and the graph of the signal generated (below).

It also allows the introduction of distortion to the signal. Baseline wander, muscular noise, power line interference and respiration noise are available in different percentages of distortion: 25%, 50% or 100% noise can be introduced into each independent lead.

3.2.2. RIGOL DG4062 Arbitrary Waveform generator

The RIGOL DG4062 is a waveform generator that can create high quality signals up to 60 MH, across two channels. It has an intuitive graphic interface.
It is not only a function generator, but an arbitrary waveform generator that includes several bio-electric signals, among which is the electrocardiography signal.

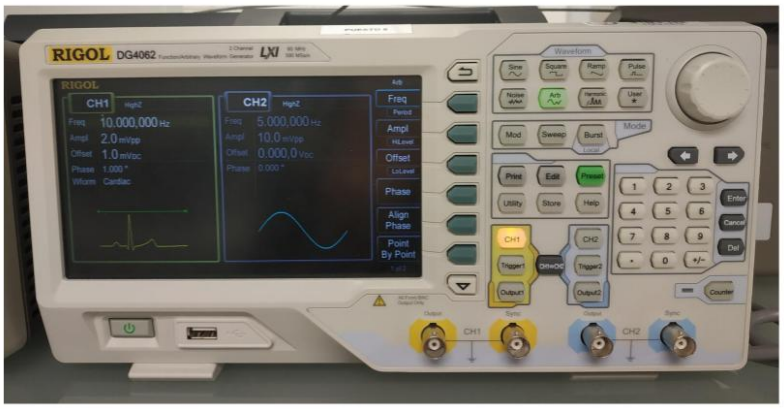

Fig. 3.9. RIGOL DG4062 Arbitrary Waveform generator

3.2.3. Measurement instruments and software tools

The Arduino open source software version 1.8.5 was used to program the device as well as uploading it to the microcontroller. The integrated development environment (IDE) compiles and uploads the program to the connected Arduino board.

For the evaluation of the correct functioning of the device, some measurement instruments and software tools have been used to assess the validity of the results.

An oscilloscope was used to visualise the analog output TTL pulse signals from the BNC cable an oscilloscope was used.

On the other hand, the processing software MATLAB 2016b was used for analysis of digital data signals, accessed through the serial monitor of the Arduino environment.

4. METHODS

4.1. Hardware implementation

The hardware of the device is centred around the interface board which connects all of the components together. This board holds the filtering circuits of all of the signals as well as the connectors that permit the mounting of the device in the box.
The signal in red in Fig.4.1 represents the voltage, supplied by an external battery. This battery is connected to the Arduino which then supplies the whole device with 5V of power. This gives the device autonomy when not connected to a computer, enabling its use in the hospital room.

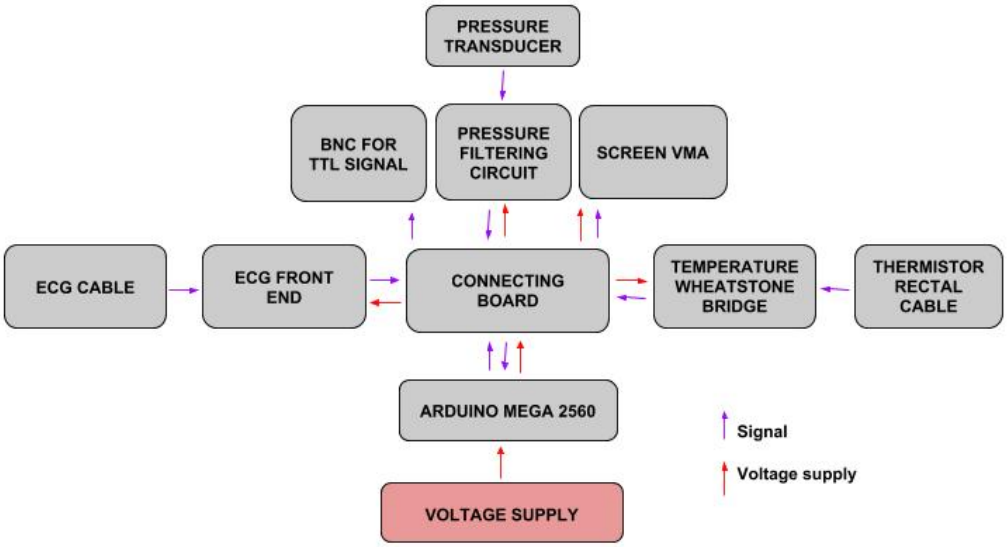

Fig. 4.1. Detailed block diagram of the device

Signals that are received by or transmitted by the micro-controller are depicted in purple, with the arrow showing the direction. The ECG front end, the pressure sensor and the temperature sensor all introduce a signal into the Arduino Mega 2560.
In turn, the TTL signal is produced by the micro-controller, and constitutes the main output of the Arduino together with all the signals that enable communication with the screen.

4.1.1. Connections and assembly

Connections and assembly are detailed in annex C.
The screen, specially designed for Arduino microcontrollers, can be fitted immediately over the device. However, to ease access to the remaining pins and facilitate the mounting process, both the screen and the microcontroller were fitted onto connectors, soldered to the adapter protoboard.

4.1.2. Cardiac signal treatment

The cardiac signal treatment was provided by the unmodified ECG front end hardware, by previously characterising both the frequency and phase response, as will be seen in chapter 5.

4.1.3. Respiratory signal detection

At the initial stages of the project, the respiratory signal was going to be implemented through the use of the impedance pneumography measurement. However this idea was abandoned in favour of a more intuitive approach, compatible with the existing hardware and setup.

Temperature sensing implementation

An initial approach to implement sensing of respiration was the placing of a thermistor immediately next to the mouse's snout, constituting a voltage divider.
The voltage divider was constructed with the thermoresistor (of approximately 1kΩ at room temperature) and a resistor of 1kΩ to assure the maximum sensitivity. This was connected to Arduino Uno and used for acquisition of the respiration signal, by the introduction of the data into MATLAB for analysis.

Final implementation: Pressure sensing

Several modes of respiratory signals were contemplated for the execution of this project, the first one being impedance pneumography. However, this diagnostic tool requires an

electric current to be supplied to the animal's body. This is harmless, but there are less invasive techniques that can supply a similar signal.

One of these less invasive methods is already implemented in *Hospital Universitario Gregorio Marañón*, and thus already proved to function in a preclinical environment, without harming the patient.

The existing equipment in the hospital consisted of a small transducer, a small sponge encased in plastic (as can be seen in Fig.4.2). When a patient is immobilised on top of the transducer, this system is able to convert the outward pressure the mouse's thoracic expansion generates, into pressure on the air inside the plastic.

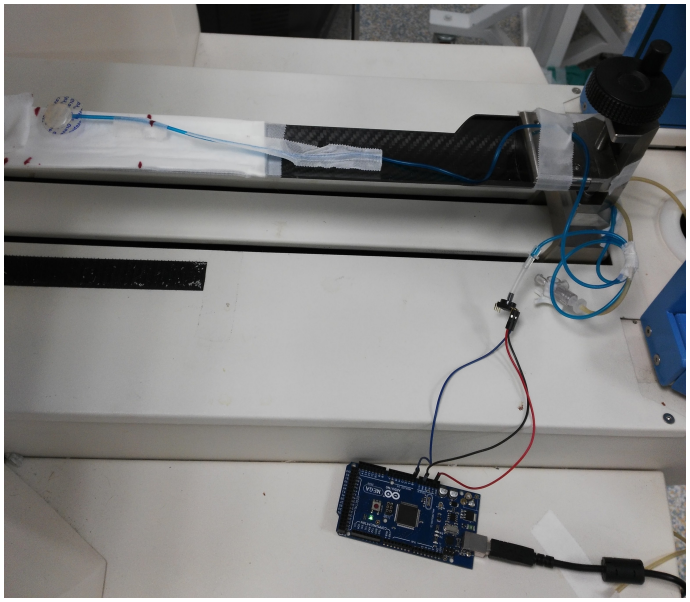

Fig. 4.2. Pressure sensor connected to preexisting hospital equipment for sensing of mouse and rat respiration during a trial with Arduino Uno.

The existing hospital system was recreated with several different sponge materials and in a range of different sizes, from 1-2 cm in diameter, to enable testing at the university laboratory. These were then compared with the existing hospital equipment, seen in Fig.4.2. To enable exchange of this transducer with the preexisting one, a *Luer* lock was connected to the tubing of the device. This way, the hospital transducer can be used, easing the setup for the user.

When tested in preclinical conditions, the raw output signal simply from the pressure sensor was inferior to the optimal range for sampling with the Arduino, therefore an

additional filtering and amplification stage seen in Fig. 4.3 was necessary.

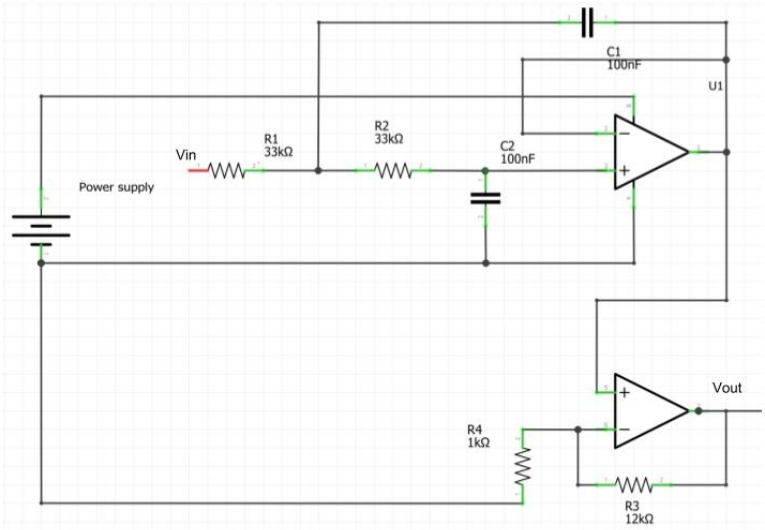

Fig. 4.3. Respiratory signal treatment. Power supply provided by Arduino

The circuit has the following components: an active low pass filter at 50 Hz to eliminate the high frequencies unnecessary for the correct sampling of the signal, followed by a non-inverting amplifier with a gain of 12. This preconditions the signal for sampling.

4.1.4. TTL signal

TTL signal is generated through an Arduino digital pin set to HIGH, generating a voltage of 5V or LOW, corresponding to a signal of 0V. This signal is then connected through a MOLEX connector to a BNC cable that feeds into the imaging machine.

4.1.5. Temperature

The implementation of the temperature sensor was chosen to be analogue because of the widely available miniaturised thermoresistors.
A Wheatstone bridge was implemented, followed by a differential amplifier to ensure good sensing of the signal. As can be seen in Fig. 4.4, the nominal value at room temperature of the thermistor is 1kΩ. The differential amplifier is specially designed to function at body temperature range.

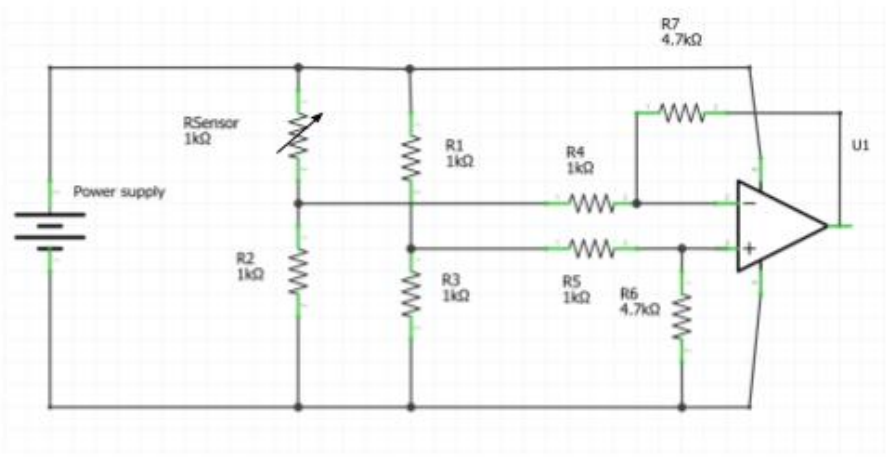

Fig. 4.4. Temperature sensing circuit, where the power supply is provided by the Arduino.

However, because of the nature of the signal, and the silicon coating needed for the rectal sensor that alters the sensitivity, a calibration of the setup was carried out. Temperature was calibrated using water at 50° C that was gradually cooled down, and measured with a thermometer. The values were obtained through the average of ten consecutive samples taken with Arduino, and conversion to voltage was not carried out for further precision in the calibration process.

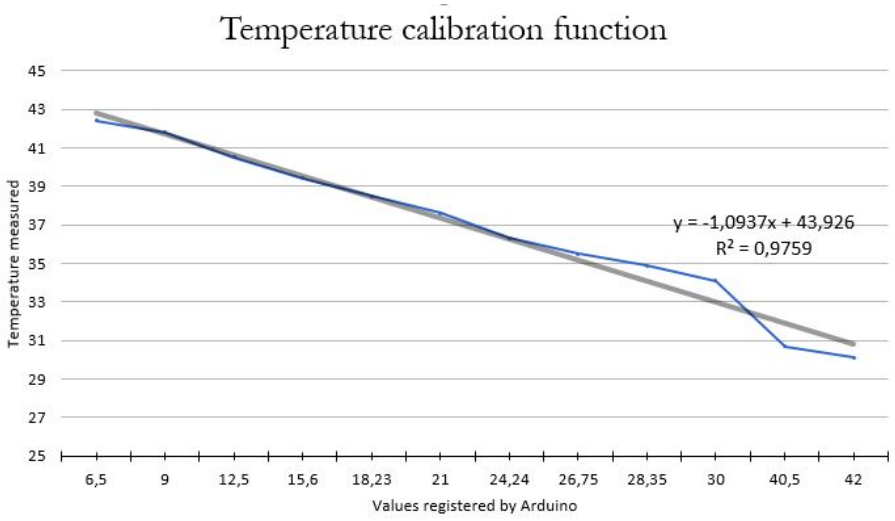

Fig. 4.5. Temperature calibration function

The calibration function depicted in Fig 4.5 fully covers the range needed for body temperature of both mice and rats.

4.2. Software implementation

The following figure (Fig. 4.6) represents the general scheme of the code which will be explained step by step.

This project requires libraries containing all the functions for the screen are needed, as well as libraries that contain the communication protocol.

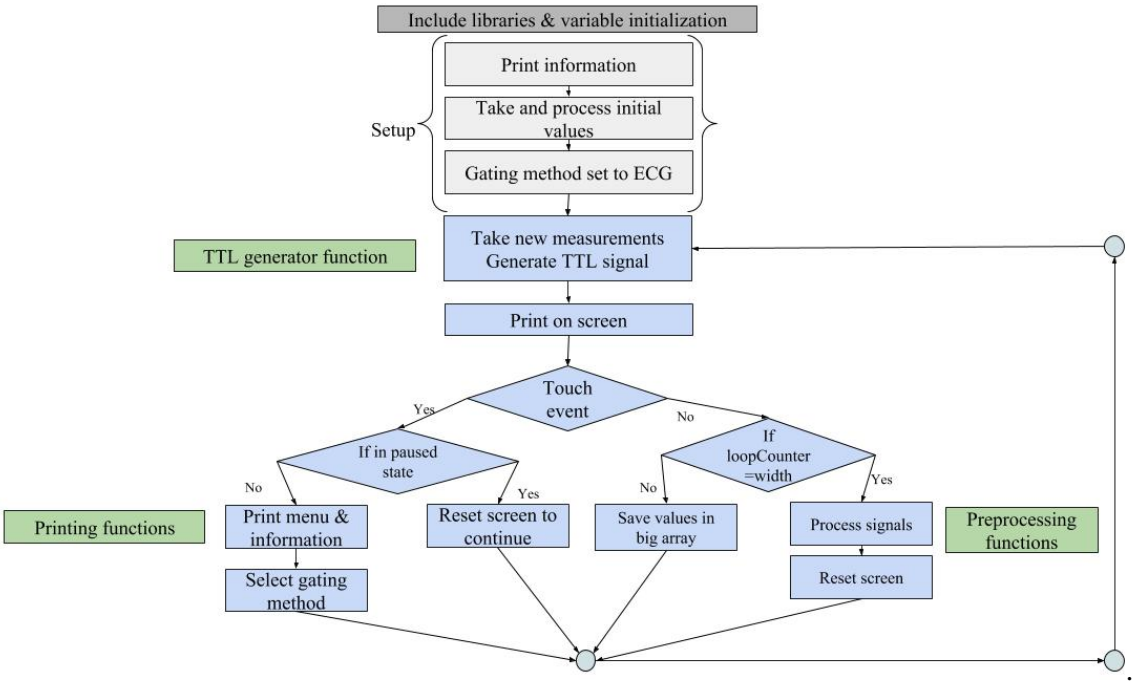

Fig. 4.6. Overview of the code used for the device. In grey, both the initialisation and the setup loop. In blue the main loop content, and in green the auxiliary functions.

All of the definitions for the display follow these initial lines of code, and all of the variables for the function of the screen are declared, such as the arrays that contain the data.

Two types of arrays were necessary for this project: a bigger array of the size of the screen (in pixels) used for the processing (as can be seen in Fig. 4.6, signals are processed for a full screen of data), and a smaller array that will permit the faster sampling of the ECG signal, to enable the TTL generation to be as real-time as possible, while sampling the respiration signal (of much lower frequency) at a lower rate.

The setup function follows these initialisations and declarations, and the machine prints the identifier of the screen's driver. While the machine is loading, initial measurements

for screen setup are performed, and values are saved as a reference for the first execution of the loop, as well as setting the screen initially for the first execution of the loop.
At the beginning of the main loop, the maximum, minimum and threshold values in each of the signals are saved for the screen representation, and new values are acquired.
The acquisitions of the signals are different depending on the frequency content: because the ECG changes much quicker than the respiration signal, the sampling is adapted. For every value in the respiration signal, three values of the ECG are taken. This allows the device to sample both signals in a more adequate way, making sure that the higher frequency signals are sampled at higher rates than those that have lower frequencies. The corresponding TTL value is calculated after each sample, making sure that it is as real time as possible, therefore three values of TTL signal are generated for each sample of the respiration signal.
To generate this TTL signal, the current value is compared to a threshold value. In the ECG, TTL is activated when the value of the signal is in the QRS complex (seen in Fig. 4.7), and in respiration, TTL is activated below a certain threshold, to ensure chest immobility (seen in Fig. 4.8). The logical *AND* of these two signals constitutes the signal corresponding to the combination of both.

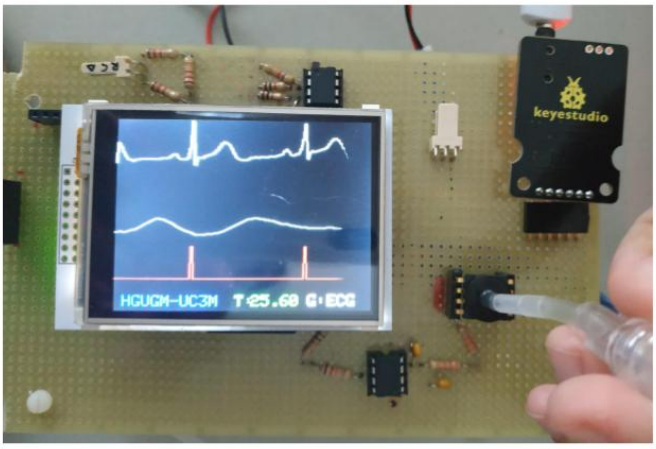

Fig. 4.7. Screen showing human ECG and simulated respiration, and TTL generated with the ECG mode selected.

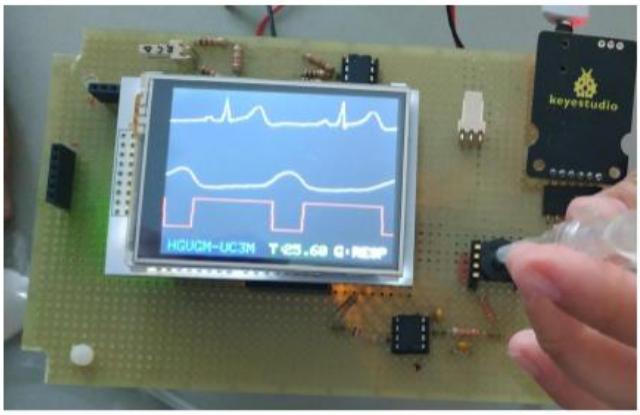

Fig. 4.8. Screen showing human ECG and simulated respiration, with TTL generated with the respiratory mode selected.

The program then checks for a touch event.
If the device was not touched previously, the menu is printed. The menu contains information about the screen and the device in general, as well as enabling the user to choose between the type of gating they prefer. By default, the chosen gating method is by using solely the ECG signal. The chosen gating method is shown at the bottom of the screen.

Fig. 4.9. Screen showing the gating menu of the device

However, if it is not the first touch event, it means that the gating menu option has been selected, and the program must restart the signal visualisation.
If there has been no touch event, values sensed are mapped to the area available for visu-

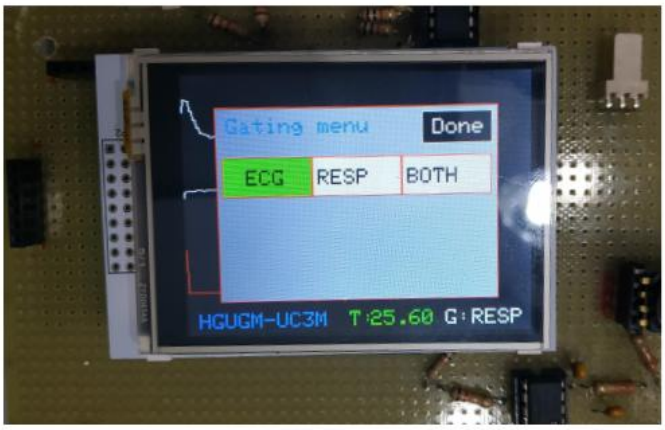

Fig. 4.10. Screen showing the gating menu of the device, with the ECG button selected.

alisation of each signal, and drawn on the screen. If there is no more space on the screen, the values saved (corresponding to the values shown on the screen) are processed: this is, the maximum and the minimum of the arrays are saved, and used for the calculation of the thresholds for the next execution of the programme.

4.2.1. Cardiac and respiratory signal processing functions

The functions implemented for the processing of the signals calculate the maximum, the minimum, and the desired threshold for the signals corresponding to the current screen: values are updated every time the screen is full of values.

4.2.2. Temperature reading and calibration functions

Temperature measurements and calibration functions are encapsulated into a single function, which is invoked every time the screen is full or the *Done* button is pressed. This value is displayed at the bottom of the screen, together with the gating method used in the current execution.

5. DEVICE EVALUATION RESULTS

5.1. System characterisation using simulated patients

5.1.1. Signal to noise ratio (SNR)

ECG signal

Two separate sinusoidal signals of 2mVpp at different frequencies were introduced through the R-lead electrode of the device for the measurements of the SNR of the ECG-FE, generated in the RIGOL DG4062 Arbitrary Waveform generator. The two remaining leads were grounded. The resulting signal, sampled by the Arduino, was then recorded in MATLAB, for further analysis.
These signals, of 1Hz and 10Hz, were analysed with Matlab's built-in SNR function, leading to significant results.
The calculations for the first signal, with a lower value of the input frequency, yield a result of 32.23 dB. The second signal, with a higher frequency of the input sinusoid, has an SNR of 29.94 dB.

Respiratory signal

In the case of respiratory signal SNR, the calculation was performed with sinusoidal signals of 500 mV at frequencies of 1Hz and 5Hz to fully model the entire the range for respiration frequencies of small animals.
These signals were introduced through the filtration circuit, to fully characterise the respiration sensing setup.
The results of this test were significant, as the SNR for the signal at 1Hz was of 27.97 dB. At 5Hz, the result of the calculation was of 25.17 dB.

5.1.2. Frequency response

The frequency response of the ECG front end was characterised by using the Pro-sim simulator, and 2 mV input signal amplitude. The frequency response (Fig. 5.1) as well as the phase response (Fig. 5.2) of the front-end filters are shown.

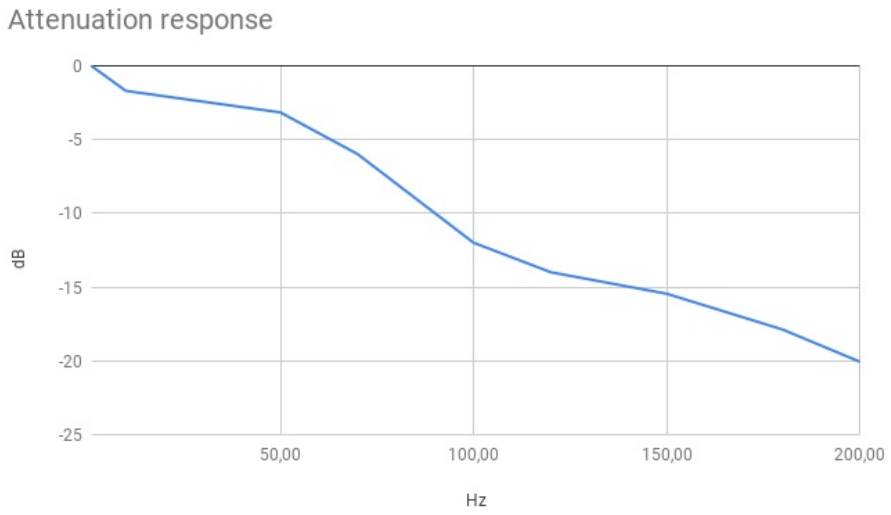

Fig. 5.1. Frequency response of the ECG sensor when a 2mV sinusoidal signal is introduced through the R lead

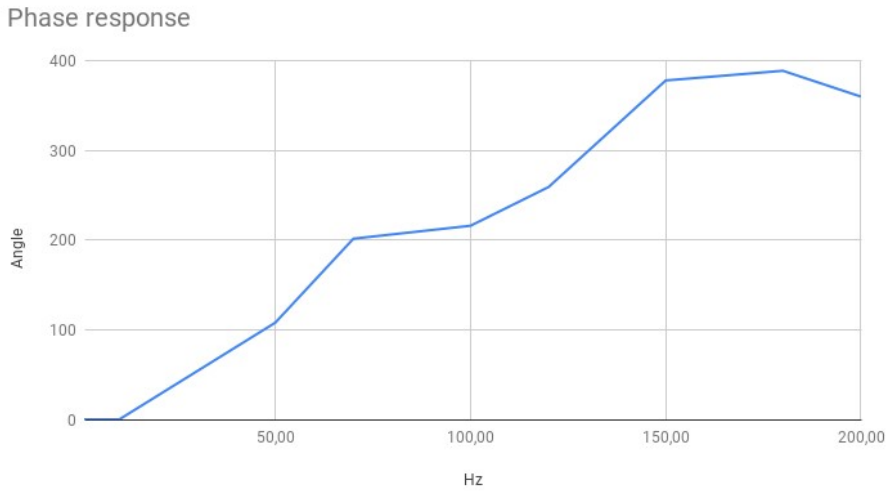

Fig. 5.2. Phase response of the ECG sensor when a sinusoidal signal with 2mV amplitude is introduced through the R lead

Because the system for respiration signal was designed in the project, the frequency

response is known and can be calculated from the circuit.

5.1.3. TTL activation

The characterization of the TTL activation was performed with two different instruments: the Pro-Sim 8 simulator and the RIGOL DG4062 Arbitrary Waveform generator. Therefore, presented in this section are results using both types of simulators.

ECG signal: Using Pro-Sim 8

A simulated cardiac signal was introduced into the oscilloscope for the testing of the TTL activation dependency on the ECG signal frequency, and compared to the output signal of the device. The reference for the signal is the QRS maximum, and the times were taken as negative for measurements taken before the maximum of the simulated signal, and positive for activations after the maximum.

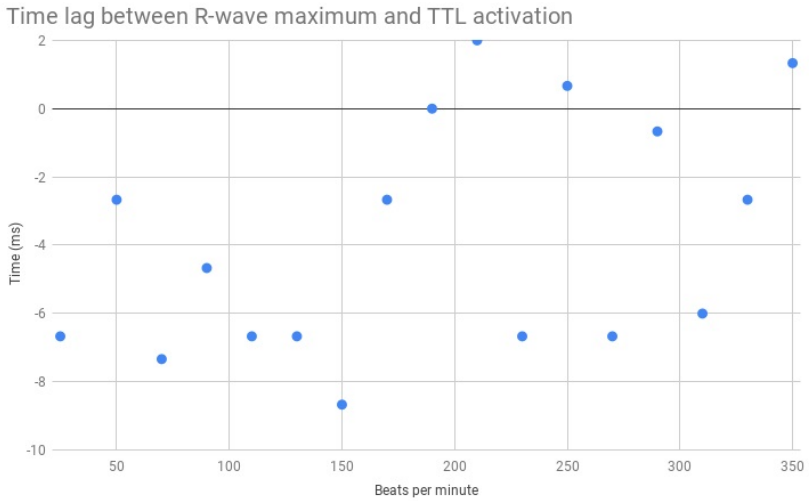

Fig. 5.3. Average time of TTL activation compared to the QRS maximum

The overall result of this test was conclusive, as the time of activation was found to have no proportionality to the heart rate: the mean time of activation was of 3.6 ms before the maximum of the R wave, and with a standard deviation of 5 ms. This mea-

surement was performed between 25 and 350 BPM, the range of the simulator. Missed beats were also quantified, and the mean of missed beats were found to be of 22%, across the same range of frequencies (25-350 BPM).

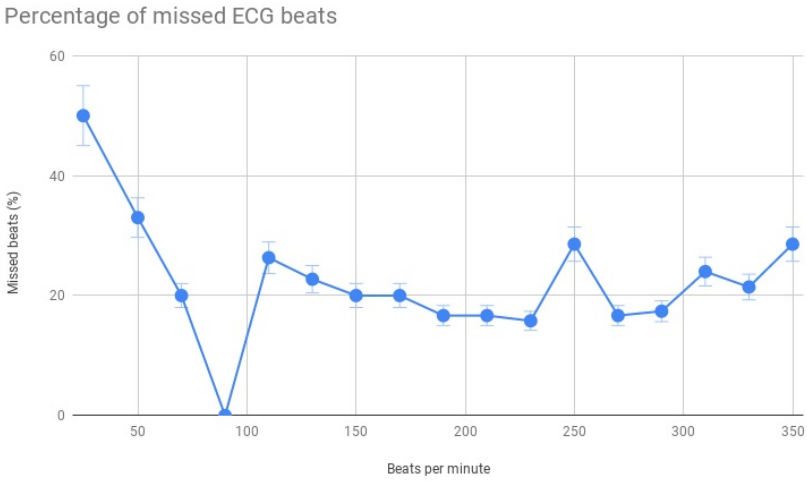

Fig. 5.4. Relationship between beats per minute of simulated ECG and percentage of missed beats in TTL

Moreover, as the artifacts in the TTL generation are dependent on the frequency of the signal. If the frequency is low, below 30 BPM, and there aren't enough QRS complexes inside a single screen, the threshold for ECG signals fail to be updated correctly, creating artifacts in the TTL activation for the ECG gating at low frequencies, as seen in Fig. 5.5.

Fig. 5.5. TTL response when a simulated 20BPM signal is put into the gating device

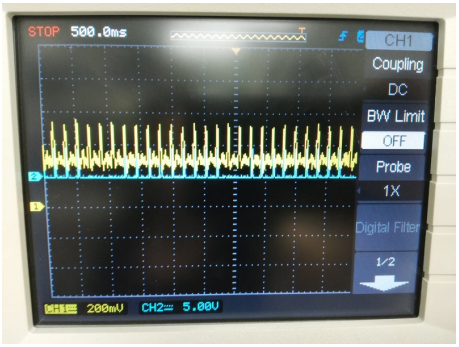

Fig. 5.6. TTL response when a simulated high frequency signal (300 BPM) is introduced into the gating device

In higher frequency simulated ECG signals, some artifacts in TTL generation can be appreciated. These artifacts coincide with the screen regeneration, the time it takes to process the signals and reset the screen to black, stops the generation of TTL output, usually fixing the value of TTL to LOW (0 V), but occasionally, the value while the screen is refreshed, is fixed to high (5 V), seen in Fig. 5.6.

ECG signal: Using a signal generator

Due to the restrictions on the range of BPM of the *Pro-sim 8 simulator*, further testing was necessary to ensure results were applicable to mouse heart rates (seen in Table 1.1). In this case, the tests were performed with simulated ECG signals obtained from the arbitrary Waveform generator, across a range of frequencies, including those of mice under anaesthesia, as this is the primary target for the device.

Across the range of frequencies tested, the distribution of the percentage of missed TTL signals appears to be dependent of frequency, as the percentage of missed QRS complexes increase slightly with an increase in frequency. The mean value of the percentage of TTL losses from 0.5 to 10 Hz is of 33,8%.

Observing the missed QRS complexes and the screen, the resetting of the screen (and therefore the time it takes to process the ECG and the respiration for the next iteration) was found to coincide with the group of missed complexes.

Occasionally, the screen will miss beats, as can be seen in Fig. 5.7.

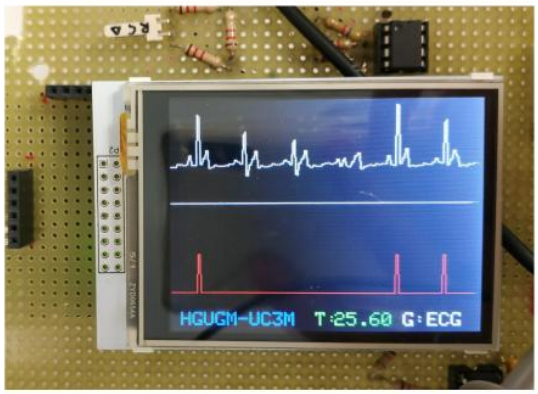

Fig. 5.7. Missed beats due to screen refresh cycle

Time lag between QRS maximum and the activation of the TTL signal was calculated in the oscilloscope. The results can be seen in Fig. 5.8.

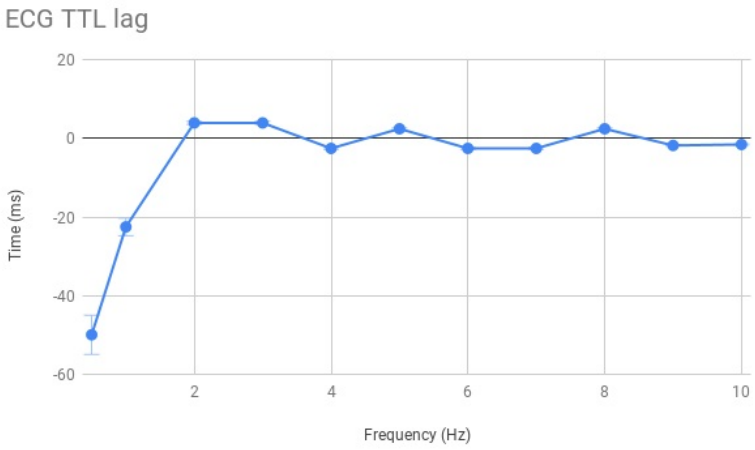

Fig. 5.8. TTL lag compared to QRS maximum, where negative indicates that the TTL activation was triggered before the R-wave maximum

The mean time lag in this frequency interval is of -6.5 ms, this indicates that the TTL activation occurs before the maximum of the QRS complex. Fig. 5.8 shows that at lower frequencies the activation occurs earlier than the R-wave maximum, however, across the frequencies needed for the monitorization of heart rate, and acquisitions of both rats and anaesthetised mice, the mean lag is of under 1 ms with respect to the R-wave maximum. The last parameter characterised in the tests with the RIGOL DG4062 Arbitrary Waveform generator was the duration of the TTL signal across the range of frequencies. Du-

ration remains consistent across the frequency range corresponding to rat and anaesthetised mouse heart rate. The mean duration of the TTL signal generated in the device in the frequency interval examined is of 25 ms.

Respiratory signal

Respiratory signal simulations were carried out with the waveform generator by inserting a 500 mVpp sinusoidal signal into the device, at the output pin of the pressure sensor, so the complete filtering and sampling process was tested.
This sinusoidal signal does not completely model the respiratory pattern of anaesthetised animals, but it is the most accurate signal that could be generated with the RIGOL simulator. The maxima in the signal correspond to the inhalations of the small animal, and the minimum of the signals correspond to the points just after exhalation.
Tests were performed between 0.3 and 5 Hz, therefore completely covering the respiratory rates of both humans and small animals.

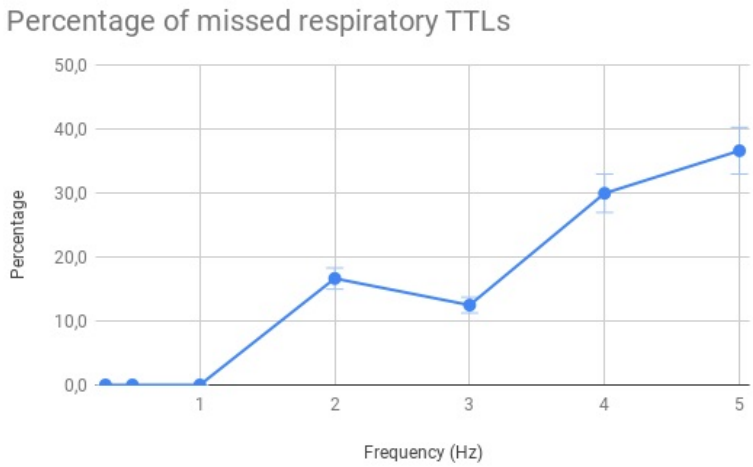

Fig. 5.9. Percentage of missed TTL activations compared to the frequency of the sinusoidal signal introduced into the device

Firstly, the amount of missed exhalations was calculated, to evaluate the dependency of the missed activations with respect to frequency. In this case, it has found to be greatly dependent of frequency, as can be seen in Fig. 5.9, the percentage of missed signal minima is proportional to the frequency introduced into the device.

The mean percentage of missed activations is of 13.7% with a standard deviation of 15% across the interval from 0,3 to 5 Hz.
However, in the interval corresponding to small animals, from 1 to 5 Hz, the mean percentage of missed activations is of 24%, with a standard deviation of 12%.

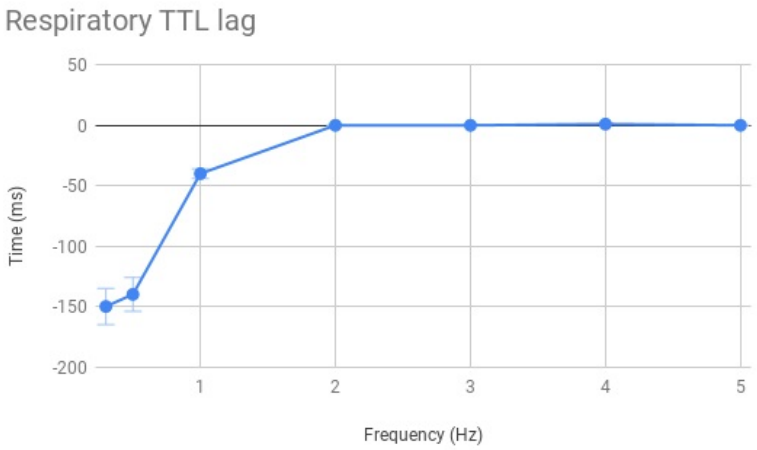

Fig. 5.10. TTL lag with respect to sinusoid minimum

The next parameter characterised was the time lag with respect to the signal minimum, because in this case, the minimum of the signal corresponds to the point just after exhalation. The results can be seen in Fig 5.11.
The mean lag across the small animal frequency interval is of -7.8 ms.

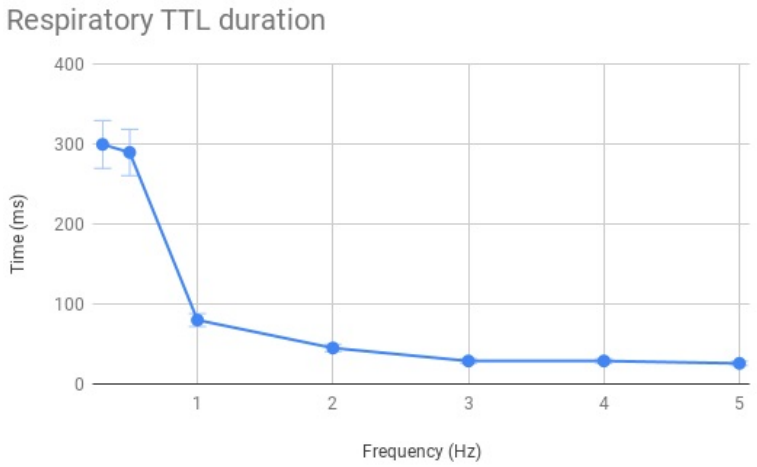

Fig. 5.11. TTL duration with respect to frequency of the sinusoid introduced

The last parameter characterised was the duration of the TTL signal. The mean dura-

tion in the interval corresponding to small animals is of 32 ms with a standard deviation of 8.7 ms.

5.1.4. Temperature measurements

During testing of the device, the temperature appearing on the screen corresponds to a stable measurement of ambient temperature, proving changes of temperature, and stable measurements when the probe was heated to body temperature.
Two time-response tests were performed with the final temperature sensor circuit, the first one was the immersion of the sensor in water at 5 °C followed by a brief introduction into water at 50 °C. Changes in voltage can be seen in Fig. 5.12.

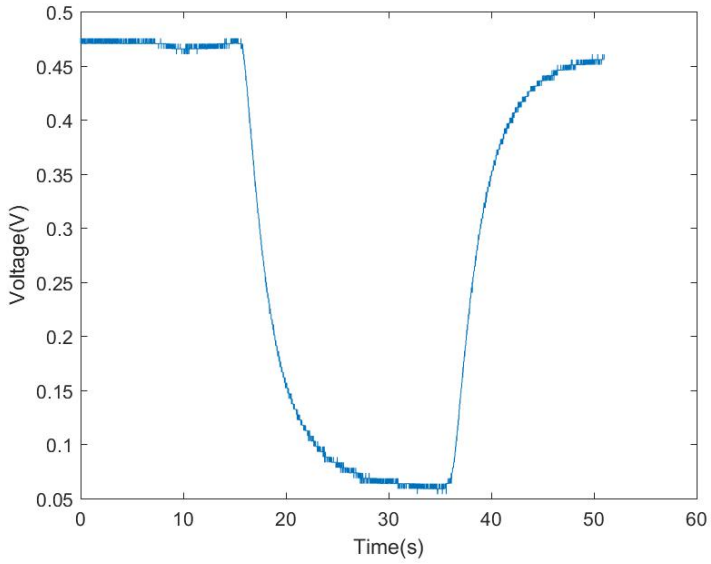

Fig. 5.12. Reaction of sensor after immersion in water at 5 °C followed by 50° C and sudden immersion into 5° C

To assess the time response and accuracy of the setup, the sensor was suddenly removed from 50° C water to find the time response of the sensor, as can be seen in Fig. 5.13.
This rate of response was considered to be sufficient for the low rate of change of the temperature signal for live animals.

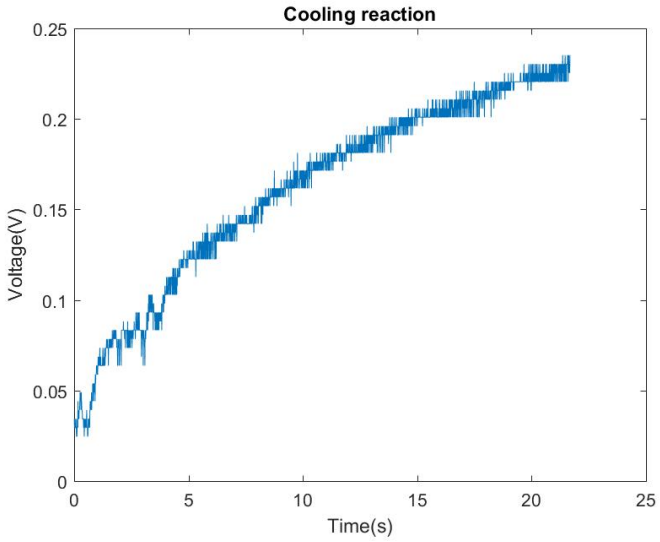

Fig. 5.13. Reaction of sensor after immersion in water at 50 °C

Because of the construction of the circuit, the signal is more accurate at temperatures under 50° C.

Temperatures of 45-50° C cause the signal in the Arduino to be unstable, as can be seen after 0-5 seconds in Fig. 5.13, because of the low Arduino input voltage, causing instabilty in the signal.

5.2. System characterisation using small animals

The system was tested at the *Laboratorio de Imagen Médica y Cirugía Experimental.* These tests were performed not only throughout the construction process, but also as a final test for the device.

Throughout the assembly phase of the device's construction, mice were used to test the limitations of the device. However, due to non-availability of mice, in the test for the final implementation, the subject used was a female rat, weighing 325 g.

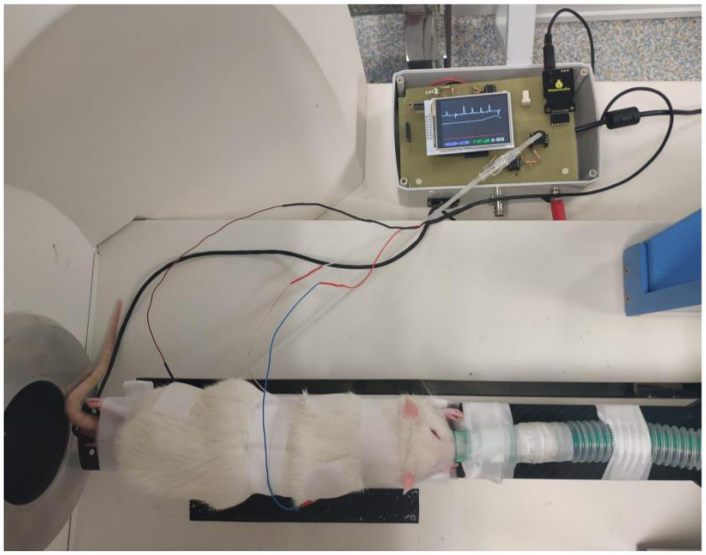

Fig. 5.14. Final testing of the device with a Wistar rat

In Fig. 5.14, the rat can be seen to have its snout completely within the tube of anaesthetic gas, composed of 100% oxygen mixed with 2.5% Sevorane. The white tape surrounding the animal not only holds both the animal and the electrodes in position, but it also presses the animal onto the transducer that will enable sensing of the respiratory signal.

The rat was hooked up to the ECG monitor with the needle electrodes made specially for this application, positioned on top of the pressure transducer, and with the rectal temperature sensor in position.

5.2.1. ECG monitor performance

The ECG monitor performance was tested as shown in Fig. 5.14. Needle electrodes were introduced subdermally, assuring the best contact possible between animal and electrode, therefore reducing impedance variability.

The signal was found to be of approximately 280 beats per minute, slightly lower than expected, probably due to the anaesthesia.

The signals obtained by sampling at 120 Hz can be seen in Fig. 5.15, where it can be seen that occasionally, the R-waves were inverted or reduced in amplitude.

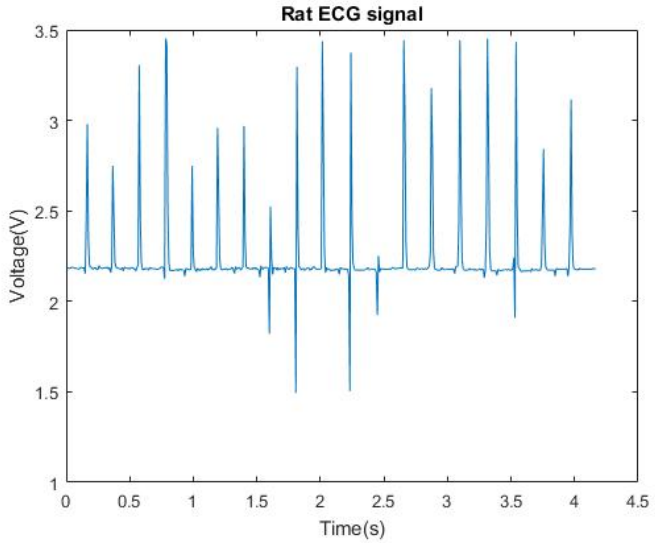

Fig. 5.15. Rat ECG signal obtained by sampling at 120 Hz

The filtered signal is in a voltage range optimal for sampling, as it is adequately amplified to a range easily introduced into the Arduino micro-controllers.

5.2.2. Respiration measurement performance

Temperature sensing implementation

As mentioned previously, in a first approach to sense respiration in mice, a temperature sensitive resistor was placed at the snout of the animal to ensure that the difference between temperature perception of inspiration and exhalation was maximum.
However, when tested at the *Hospital General Universitario Gregorio Marañón* with small animals, the system did not provide a suitable signal under preclinical conditions, as the slight differences in temperature caused by inhalation and exhalation cannot be appreciated due to the continuous flow of anaesthetic gas into the snout of the animal during a procedure.

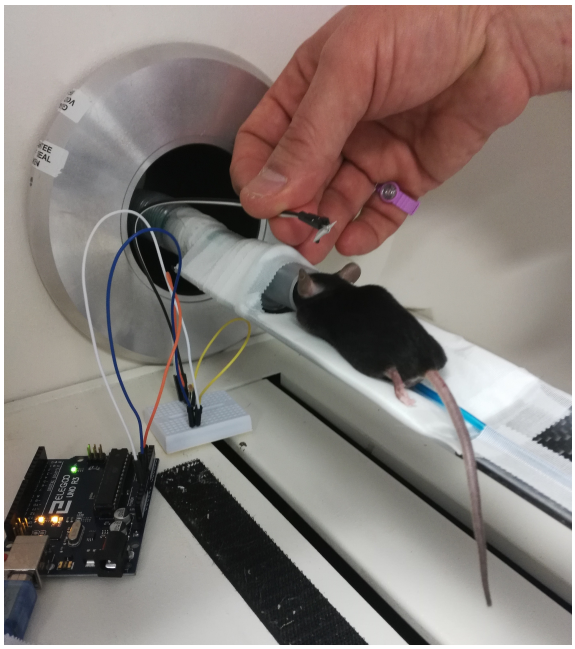

Fig. 5.16. Thermistor respiration sensing implementation

Final implementation: Pressure sensing

The final implementation chosen for the sensing of respiration signals was the sensing through the use of a pressure sensor, as discussed previously.
In this case, the output signal needed to be filtered in order to detect it in the Arduino, adapting the signal range to that of sampling with the microcontroller.

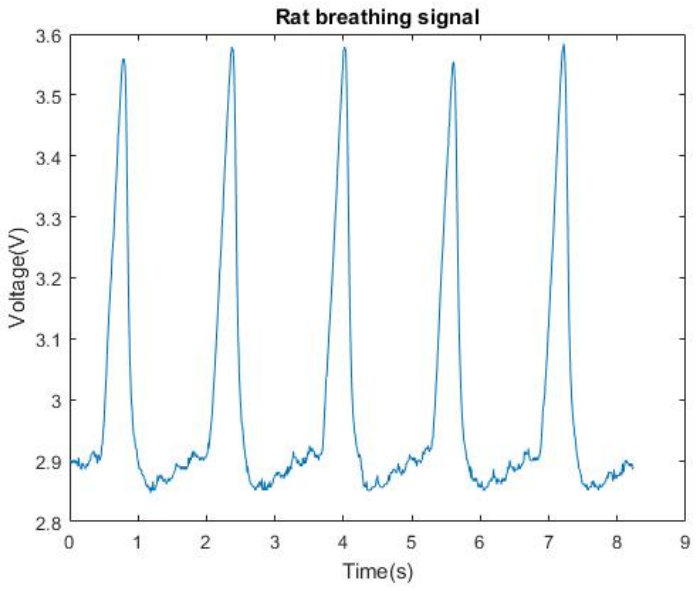

Fig. 5.17. Respiration signal obtained by sampling at 120 Hz

As seen in Fig. 5.17, the range of the signal was correctly adapted to the voltage range needed for sampling.

In the initial stages of the project, the transducer already used at the hospital was compared to the transducer specially made for the simulated tests, and they were found to have similar output signal characteristics.

However, it is worth mentioning that the transducer used in these tests was the one specially manufactured for the simulations (seen in 3.5.), instead of the one already present in the *Laboratorio de Imagen Médica y Cirugía Experimental* at Gregorio Marañón Hospital, as the transducer currently there was being used in another procedure.

5.2.3. TTL activation

For TTL activation results, the three activation modes were qualitatively analyzed by the hospital staff, and sample screens are shown below, the ECG activation, seen in Fig. 5.18, followed by respiratory gating (Fig. 4.8), and the generation of the signals through the combination of both signals, seen in Fig. 5.20.

The performance of the ECG mode had certain constraints, caused by the artifacts in QRS complexes. However, the algorithm was able to generate the output TTL signal in approximately 80% of the R-waves on the screen.

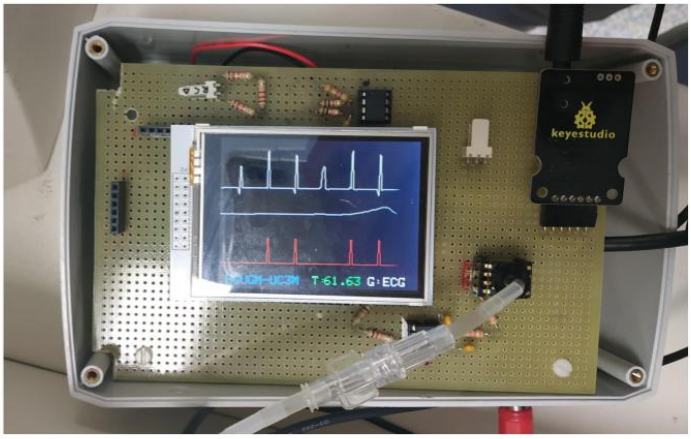

Fig. 5.18. Cardiac gating

Respiratory gating of the signal was also tested. As seen in Fig. 5.17, the frequency is much lower than those anticipated in the laboratory and therefore the device had no

problem sensing the respiratory signal.

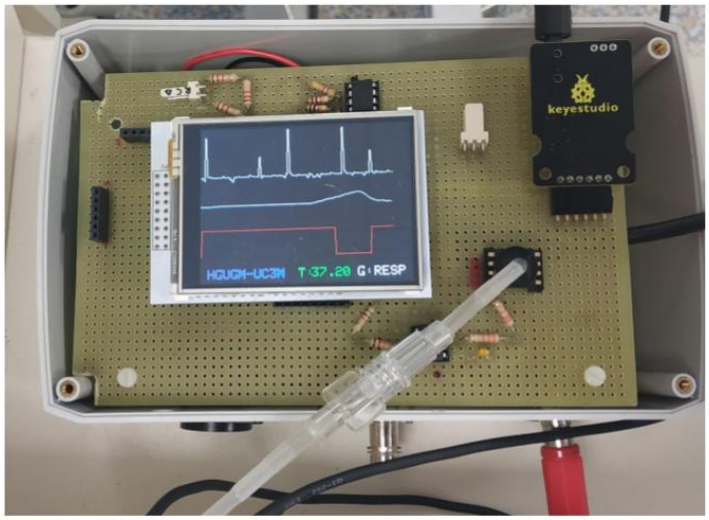

Fig. 5.19. Respiratory gating

The combination of both signals into a single TTL output was also tested, to ensure the correct function of the gating mode. In Fig. 5.20, the machine can be seen to eliminate one of the undesired QRS signals because of chest movement due to respiration.

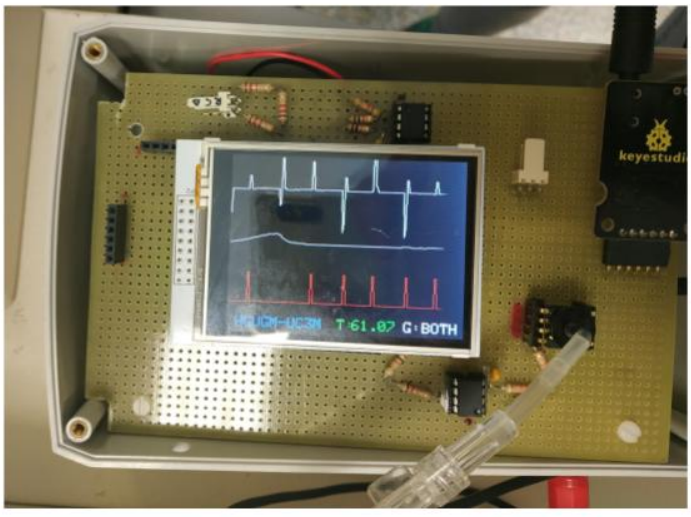

Fig. 5.20. Gating with a combination of ECG and respiration signals

Overall, the gating algorithm was shown to work in the preclinical setting.

6. DISCUSSION AND CONCLUSIONS

The main objective of this project was to make a medical device that allowed simultaneous monitoring of the ECG and the respiration signal of small animals, as well as providing an adequate gating signal for the Argus PET/CT machine of the *Laboratorio de Cirugía Experimental* at the *Hospital General Universitario Gregorio Marañón.*
This section examines both the function and functionality performance of the device. By analysing both the behaviour and execution of the device and the usability of the device respectively, it will assess whether the main objective and its further goals have been fulfilled.

6.1. Device function

The results of the device evaluation are convincing, because thorough laboratory testing has been performed on the overall device, as well as testing in a real preclinical environment. The results show that the device has an adequate behaviour for its purpose.
The Signal-to-noise ratios, a commonly used measurement of a signal's quality, prove that the filtering components are functioning correctly, providing a clean signal to the device in the range of frequencies tested. These results show that this device has a cleaner signal than those of the previous works[32] [33].
To assess the amplitude and frequency responses, the ECG front end was tested with the arbitrary waveform generator. However, these results (Fig. 5.1 and Fig. 5.2) do not completely represent the reality of the response, as these tests were performed with the RIGOL waveform generator, equipment not specially designed for such low amplitude signal generation (as previously mentioned, the signal used had an amplitude of 2mV). Therefore, the signal introduced into the device was already one of low SNR, and the tests could not be performed with a greater amplitude, as this parameter was chosen according to the gain introduced by the ECG-front end, otherwise the results could not be properly obtained due to clipping.
In relation to the TTL activation tests, the results were as expected, as the TTL activation percentage was not expected to be perfect. However, when observing the output of the

device with respect to introduced QRS complexes, the source of the problem was found to be the time it takes for the screen to reset. This causes the device to stop sampling the signals and therefore it interrupts the generation of TTL output.

Occasionally, the device is not able to correctly sample the cardiac signal, as seen Fig. 5.7. This is due to the time it takes for the microcontroller to communicate with the screen: the process of printing the signal causes the device to miss an occasional QRS complex.

Two different simulators were used for the ECG signal, the Pro-Sim 8 was selected due to its high quality signal output and multiple options for ECG generator, but its heart rate limitation (from 10-360 BPM) was the motivation for searching for another instrument that would allow for the simulation of bio-electrical signals across the frequency range needed for both rats and anaesthetised mice [28] [16].

Tests with simulated respiration are unconvincing, as the sinusoid was the closest simulation that could be made of the respiratory signal, but it was not realistic enough, as seen in Fig. 5.17, so further studies should be carried out to fully characterise the system.

Overall, the gating algorithm has been shown to generate TTL signals with sufficient accuracy under laboratory conditions, in a range of frequencies suitable for rat and anaesthetised mice simulation.

As for the tests in the preclinical setting, results were also conclusive: the final arrangement of the device is adequate for the generation of a gating signal for rats, and is significantly better than that of previous work [33].

Small animal respiration signal acquisition was found to be completely satisfactory. The gating algorithm proved successful in the tests, and the filtration was found to be correctly performed.

The needle electrode length and placement was found to be responsible for the negative QRS complexes seen in Fig. 5.15, Fig. 5.18, Fig. 5.19 and Fig. 5.20, as small movements could cause an impedance difference that could lead to the negative signals.

However, the intention of this device was not to provide a diagnosis-grade ECG reading, but QRS detection, and the quality of the signal is sufficient for this use, as more than 80% of the QRS complexes were seen to be detected (see Fig. 5.18, Fig. 5.19 and Fig. 5.20). The quality of the signal is also comparable to that obtained in previous works [33].

The overall conclusion concerning the device function is that with the exception of a

tolerable percentage of missed TTL activations which will be addressed in future work, the device was shown to comply with the objectives proposed for this bachelor thesis.

6.2. Device functionality

The functionality of the device described in this bachelor thesis was tested with simulated patients and in a real clinical environment, with both leading to satisfactory results. However, the main functionality assessment of the device was performed at the *Laboratorio de Imagen Médica y Cirugía Experimental*, where the technicians and researchers were favourably impressed with the ease of use of the device and its intuitive interface. The creation of a touchscreen interface has greatly advanced the device by introducing the possibility of selecting a gating mode specific to the application needed. The screen algorithm was also perfected to enable the correct visualisation of an adequate duration of the signals, as well as the current gating mode display.

The temperature sensor was miniaturised with respect to the previous project, easing application in a real clinical environment, thereby improving the functionality of the overall device [33].

Technicians' opinion of the concept of the introduction of the "Luer" lock was also favourable, as it would ease the implementation of the device, and make the existing hardware more portable.

This device for image gating provides a solution for a current issue at the *Hospital Universitario Gregorio Marañón*, and its implementation will ease acquisition and monitorization on an everyday basis, helping to reduce thoracic motion, one of the most common issues in current cardiac imaging techniques.

6.3. Current device status

The prototype proposed in this bachelor thesis has provided substantial improvements with respect to the previous device, the most notable of which is the addition of the respiratory signal for better motion reduction during acquisition. This addition has greatly changed device architecture, as well as functionality, requiring a touchscreen interface for selection of gating methods.

This improvement of the previous device means an enhancement of the overall function and functionality with respect to previous prototypes, with a cleaner ECG signal (although not one of the primary objectives of the thesis, always desirable), the addition of respiration for the execution of a portable device with full vital sign monitorization, more reliable TTL signal activations, and a wider range of activation options.

When tested in a real clinical environment, the device was shown to properly analyse the real ECG and respiratory signal of the rat, and correctly produce the TTL signals. The device was also found to be intuitive and easy to use by the staff at the Hospital.

However, the device possesses certain constraints, the most prominent one being the absence of a percentage of the TTL activations, due to the screen refresh, something that can be estimated in post-processing, but is among the constraints that will be addressed in future work. Further work should include the evaluation of the device to adjust the generated TTL signal to allow for the correct detection of the signal by the Argus PET/CT.

6.4. Future improvements

Even though the overall results of the device are satisfactory, there are several aspects that could enhance the device, described in the following section.

The first improvement would be the modification of the ECG acquisition electronics, as the ECG-FE's filtering stage could be further adapted to the final subjects, ensuring a better filtering for each of the target small animal species, and resulting in an improved signal processing, and an improved device function.

The hardware implementation of the device, although currently reliable, could be redesigned into a PCB to ease assembly and minimise electrical interferences, as well as

providing a more reliable power supply to all of the components on the protoboard.
Another issue that should be addressed is the redesign the algorithm for detection and triggering of the TTL signal. The current algorithm causes the device to miss some beats with the screen refresh, a problem that can be easily solved in post-processing of the images taken with retrospective gating. However, the algorithm should be redesigned to minimise the time employed on the screen refresh.
However, having in mind the final use of the device, there are several modifications that could be introduced that could solve the screen issues.
Technicians need the ECG signal for monitorisation, so a possible solution to the screen issue would be to use LED lights and/or sound to show both ECG and respiration. Therefore the screen could be left for the setup of the procedure (to ensure the right positioning of the electrodes and transducer) and for interface with the user, for gating mode selection.

6.5. Scientific and social impact

The satisfactory results of this project could have interesting outcomes for science and society.
First of all, the miniaturisation and portability implemented in this device enable vital sign monitorization of small animals everywhere, with an easy to use interface. It requires no previous training and can therefore be used in any preclinical research environment.
Devices such as the one developed in this thesis constitute an easier and more intuitive application of the gating techniques. They allow a combination of vital signs to produce a single gating signal, increasing the accuracy, and easing the process of cine-cardiac study acquisition, as well as simplifying the process of the acquisition of such studies by taking measurements of as few parameters as possible without eliminating functionality.
With the use of devices such as this one, image acquisitions containing noise due to chest movement can be greatly reduced and therefore image quality could be greatly enhanced, reducing the need for repeated images.
Even though there are several ways of performing gating, this device is unique in that

it will help the *"Laboratorio de Imagen Médica"* of the *"Hospital Gregorio Marañón"*, by being specially designed for use with their existing respiration measurement setup, thus easing the transition between the previous device and the one presented in this work.
The estimation of material costs for this device is under 200€ (detailed in the budget). This means that even though the final cost of the device would be higher due to additional factors, the cost would still be under 300€. This proves a significant price reduction not only with respect to the market, but also with respect to the previous thesis [33]. This would make it an interesting candidate for introduction into the market, provided the adequate business case is prepared.
This device could also have many other uses, the most important of which could be the use of a similar device to improve the current method for application of radiotherapy inside the thoracic cavity, mainly lung cancer. This could also be implemented in any other applications that require the absence of motion.
The present device could be used with any imaging modality, even though for some of the techniques it would have to undergo several modifications. This device, given several minor modifications and corresponding regulatory marking could also be applied for use in humans.

7. BUDGET

This section details the estimated time invested in this project as well as its cost (Table 7.5): personnel cost is broken down in Table 7.1, material costs (Table 7.2), as well as the charges incurred during testing at *Gregorio Marañón Hospital*, in Table 7.3.

7.1. Personnel cost

The time dedicated to the project by the biomedical engineer was of approximately 700 hours. Also included are the hours dedicated by the project manager, for supervision and guidance. A laboratory technician was required mostly for the training stage as well as assistance with assembling the device.

Role	Time (hrs)	Hourly cost	Total cost(€)
Project manager	100	40	4000
Laboratory technician	100	18	1800
Biomedical Engineer	700	20	14000
Total personnel cost			**19800**

TABLE 7.1. PERSONNEL COST FOR THE PROJECT

7.2. Material cost

The materials needed for this project provide an additional source of cost, deriving mainly from the purchase of the components of this device.

Item	Cost(€)
Arduino MEGA 2560	41,50
AD8232 ECG FE	14
VMA412 tft screen	28
Adapter protoboard	10
P1K0.161.1E.A.040 (Temperature sensor)	18
MPXV5010GC7U (Pressure sensor)	13
Electronic components	1,10
Additional components (connectors, cables...)	30
Total cost	**155,6**

TABLE 7.2. MATERIAL COST WITH VAT INCLUDED

7.3. Service cost

The service costs were calculated according to the current costs of the "Laboratorio de imagen para pequeño animal de experimentación" that can be found linked here

Concept	Cost per hour	Time (hrs)	Total cost(€)
Electronic assembly workshop	10	30	300
PET/CT	120	5	600
Anaesthesia	10	5	50
Imaging technician	17	5	85
Total service cost			**1035**

TABLE 7.3. SERVICE COST

7.4. Software licenses

Concept	Yearly cost	Months of use	Total cost(€)
Matlab license	1200	1	100

TABLE 7.4. SOFTWARE LICENSE

7.5. Overall cost

Therefore the overall cost can be seen in the following table

Concept	Total cost(€)
Personnel cost	19.800
Material cost	155,6
Service cost	1.035
Software license	100
Direct cost subtotal	**21.090,6**
Indirect cost(15%)	3.163,59
Industrial benefit(6%)	1.265,44
VAT (21%)	**5.259,12**
Total cost	**30.878,75**

TABLE 7.5. OVERALL COST OF THE PROJECT

BIBLIOGRAPHY

[1] R. H. Anderson, R. Razavi, and A. H. Taylor, "Cardiac anatomy revisited", *Journal of Anatomy*, vol. 205(3), pp. 159–177, 2004.

[2] N. J. Ashley EA. (). Cardiology explained., [Online]. Available: https://www.ncbi.nlm.nih.gov/books/NBK2214/. (accessed: 07.09.2018).

[3] J. Zimmerman, "The functional and surgical anatomy of the heart", *Annals of The Royal College of Surgeons of England*, 1966.

[4] Wapcaplet. (). Diagram of the human heart, [Online]. Available: https://commons.wikimedia.org/w/index.php?curid=830253. [CC BY-SA 3.0] (accessed: 08.09.2018).

[5] D. Ho, X. Zhao, S. Gao, C. Hong, and D. Vatner, "Heart Rate and Electrocardiography Monitoring in Mice", *Current Protocols in Mouse Biology*, pp. 123–139, 2011. DOI: http://doi.org/10.1002/9780470942390.mo100159.

[6] M. AlGhatrif and J. Lindsay, "A brief review: History to understand fundamentals of electrocardiography", *Journal of Community Hospital Internal Medicine Perspectives*, vol. 2(1), 2012.

[7] L. W. &. Wilkins, *ECG Interpretation Made Incredibly Easy*, 2005. DOI: 10.5005/jp/books/10248. [Online]. Available: http://books.google.com/books?id=mGiTP7zCHUAC%7B%5C&%7Dpgis=1.

[8] A. Atkielski. (). Sinus rhythm labels, [Online]. Available: https://commons.wikimedia.org/wiki/File:SinusRhythmLabels.svg. (accessed: 23.08.2018).

[9] N. Patchett. (). The limb leads and augmented limb leads, [Online]. Available: https://commons.wikimedia.org/w/index.php?curid=39235282. [CC BY-SA 4.0] (accessed: 08.09.2018).

[10] J. Pan and W. J. Tompkins, "A Real-Time QRS Detection Algorithm", *IEEE Transactions on Biomedical Engineering*, vol. BME-32, no. 3, pp. 230–236, 1985. DOI: 10.1109/TBME.1985.325532. [Online]. Available: http://ieeexplore.ieee.org/document/4122029/.

[11] H. Limaye and V. V. Deshmukh, "ECG Noise Sources and Various Noise Removal Techniques: A Survey", *International Journal of Application or Innovation in Engineering & Management*, no. 2, pp. 2319–4847, 2016.

[12] S. P. Aswathy Velayudhan. (). Noise analysis and different denoising techniques of ecg signal - a survey, [Online]. Available: http://www.iosrjournals.org/iosr-jece/papers/ICETEM/Vol.%201%20Issue%201/ECE%2006-40-44.pdf. (accessed: 07.09.2018).

[13] V. H. Kramer K. van Acker S.A., "Use of telemetry to record electrocardiogram and heart rate in freely moving mice", *Journal of Pharmacological and Toxicological Methods*, vol. 30, no. 4, pp. 209–215, 1993. DOI: https://doi.org/10.1016/1056-8719(93)90019-B.

[14] W. Erhardt, A. Hebestedt, G. Aschenbrenner, B. Pichotka, and G. Blümel, "A comparative study with various anesthetics in mice (pentobarbitone, ketamine-xylazine, carfentanyl-etomidate)", vol. 184, pp. 159–69, Feb. 1984.

[15] T. M. Fleming S. (). Normal ranges of heart rate and respiratory rate in children from birth to 18 years: A systematic review of observational studies., [Online]. Available: http://doi.org/10.1016/S0140-6736(10)62226-X. (accessed: 07.09.2018).

[16] J. H. University. (). Species-specific information: Mice, [Online]. Available: http://web.jhu.edu/animalcare/procedures/rat.html. (accessed: 07.09.2018).

[17] B. S. Chaudhry R. (). Anatomy, thorax, lungs., [Online]. Available: https://www.ncbi.nlm.nih.gov/books/NBK470197/. [Updated 2017 Dec 15] (accessed: 08.09.2018).

[18] J. D. Tobias, "Conventional mechanical ventilation", *Saudi Journal of Anaesthesia*, no. 4(2), pp. 86–98, 2010.

[19] Cruithne9. (). The muscles of quiet breathing, [Online]. Available: https://commons.wikimedia.org/w/index.php?curid=59895132. [CC BY-SA 4.0] (accessed: 23.08.2018).

[20] F. Q. Moody, R. Saatchi, D. Burke, H. E. Elphick, and S. Tan, "Rate monitoring methods: A review.", *Pediatric Pulmonology*, vol. 46 (6), pp. 159–177, 2011.

[21] T. C. Poder and K. L. Ewing, "Brief Note Impedance Pneumography in Mice : Electrode Design and the Effect of Electrode Location", *Ohio Journal of Science*, vol. 78, no. 2, pp. 82–85, 1978.

[22] M. Młyńczak and G. Cybulski, "Impedance pneumography: Is it possible?", vol. 8454, 84541T, 2012. DOI: 10.1117/12.2000223. [Online]. Available: http://proceedings.spiedigitallibrary.org/proceeding.aspx?doi=10.1117/12.2000223.

[23] W. J. G. Luo S. Afonso V. X., "The electrode system in impedance-based ventilation measurement", *IEEE Transactions on Biomedical Engineering*, 1992.

[24] G. B. Moody, R. G. Mark, A. Zoccola, and S. Mantero, "Derivation of respiratory signals from multilead ecgs", *Computers in Cardiology*, vol. 12, Jan. 1985.

[25] A. Singh and A. Chaudhary, "Real Time Respiration Rate Measurement Using Temperature Sensor", pp. 605–607,

[26] C. M. Zehendner, H. J. Luhmann, and J.-W. Yang, "A simple and novel method to monitor breathing and heart rate in awake and urethane-anesthetized newborn rodents", *PLOS ONE*, vol. 8, no. 5, pp. 1–9, May 2013. DOI: 10.1371/journal.pone.0062628. [Online]. Available: https://doi.org/10.1371/journal.pone.0062628.

[27] M. M. Kabir *et al.*, "Respiratory pattern in awake rats: Effects of motor activity and of alerting stimuli", *Physiology & Behavior*, vol. 101, no. 1, pp. 22–31, 2010. DOI: https://doi.org/10.1016/j.physbeh.2010.04.004. [Online]. Available: http://www.sciencedirect.com/science/article/pii/S0031938410001629.

[28] J. H. University. (). Species-specific information: Mice, [Online]. Available: http://web.jhu.edu/animalcare/procedures/mouse.html. (accessed: 07.09.2018).

[29] B. Desjardins and E. A. Kazerooni, "ECG-Gated Cardiac CT", *American Journal of Roentgenology*, no. April, pp. 993–1010, 2004.

[30] A. Ellster. (). Gating vs triggering, [Online]. Available: http://mriquestions.com/gating-v-triggering.html. (accessed: 07.09.2018).

[31] A. Ellster. (). Gating methods, [Online]. Available: http://mriquestions.com/gating-methods.html. (accessed: 07.09.2018).

[32] B. Velasco Regúlez. (). Dispositivo de monitorización de la señal cardíaca de pequeño animal de laboratorio para la adquisición de imágenes médicas con sincronismo cardíaco, [Online]. Available: https://e-archivo.uc3m.es/handle/10016/24833. (accessed: 23.08.2018).

[33] I. M. García López. (). Programming and testing of a small-size ecg monitor for small animal gated imaging, [Online]. Available: https://e-archivo.uc3m.es/handle/10016/23443. (accessed: 23.08.2018).

GLOSSARY

BPM Beats per minute. xvi, 7, 39, 40

CPM Cycles per minute. 11

CT Computed tomography. 13, 16

ECG Electrocardiogram. iii, 2, 13

EDR Electrocardiogram (ECG) derived respiration. 9

FE Front end. iii

PET Positron emission tomography. 13

PWM Pulse width modulation. 20

SNR Signal to noise ratio. 36

TFT Thin Film Transistor. 19

TTL Transistor-transistor logic. 13

VAT Value added tax. xvi, 58

ANNEX A: HUMAN AND RODENT BODY TEMPERATURES

The body temperatures of humans, mice and rats are all detailed in the table below.

	Temperature range
Human	36.5 - 37.5 °C
Rat [16]	35.9 - 37.5 °C
Mouse [28]	36.5 - 38 °C

ANNEX B: BUILD OF MATERIALS (BOM)

Quantity	Module
1	Arduino MEGA 2560 microcontroller
1	USB A-B cable
1	USB A-A cable
1	AD8232 ECG FE by Keyestudio
1	VMA412 touchscreen by Velleman
1	P1K0.161.1E.A.040 temperature sensor
1	MPXV5010GC7U pressure sensor
10	Resistors of several values
2	Capacitors
2	LMC6482IN Operational amplifiers
3	MOLEX connectors
1	Luer lock
2	Medical grade (IV) tubes
1	Male stereo Jack connector
1	Male and female RCA connector
1	Female BNC connector
1	USB A-A female connector
1	9V battery
1	Switch
1	RETEX ABS box
1	"Wire Wrap" wire spool
1	Double coaxial cable spool

ANNEX C: PINOUT CONNECTIONS

In the table below, connections for the different modules of the device can be seen.

Device	Connection	Arduino Mega 2560 pin
ECG-FE	Vin(ECG)	10
	LO+	42
	LO-	44
	Power supply	3.3V
	GND	GND
Pressure sensor	Vin(P)	9
	Power supply	5V
	GND	GND
Temperature sensor	Vin(T)	8
	Power supply	5V
	GND	GND
TTL	TTLSignal	32

ANNEX D: SCHEMATICS AND DATASHEETS

In this annex, the datasheets and the schematics for the components used can be found:

Arduino MEGA 2560

Schematic for Arduino Mega 2560

Schematic for pin mapping for the Atmega2560

Arduino2560 user manual

ECG Front end

Ks0261 keyestudio AD8232 ECG Measurement Heart Monitor Sensor Module

VMA412 screen

VMA412 User Manual

VMA412 Diagram

Temperature sensor

P1K0.161.1E.A.040 temperture sensor datasheet

Pressure sensor

MPXV5010GC7U pressure sensor technical datasheet